Geodesy and Geodynamics xxx (xxxx) xxx

Contents lists available at ScienceDirect

Geodesy and Geodynamics

journal homepage: http://www.keaipublishing.com/geog

Temporal variations in coda attenuation associated with the 2008 Wenchuan (M_W7.9) Earthquake in SW, China

Junhua Hu [a, b, *, 1], Guoxin Zhang [a, b], Liyun Fu [c], Yan Zhang [d, e, f], Songhui Li [a, b]

[a] State Key Laboratory of Simulation and Regulation of Water Cycle in River Basin, China Institute of Water Resources and Hydropower Research, A-1 Fuxing Road, Beijing 100038, China
[b] Department of Structures and Materials, China Institute of Water Resources and Hydropower Research, A-1 Fuxing Road, Beijing 100038, China
[c] Key Laboratory of Deep Oil and Gas, China University of Petroleum (East China), Qingdao 266580, China
[d] Key Laboratory of Earth and Planetary Physics, Institute of Geology and Geophysics, Chinese Academy of Sciences, No. 19, Beitucheng Western Road, Beijing 100029, China
[e] University of Chinese Academy of Sciences, Beijing 100049, China
[f] Innovation Academy for Earth Science, Chinese Academy of Sciences, No. 19, Beitucheng Western Road, Beijing 100029, China

ARTICLE INFO

Article history:
Received 16 March 2021
Accepted 6 September 2021
Available online xxx

Keywords:
Wenchuan earthquake
Single-scattering model
Coda attenuation
Tectonic static stress

ABSTRACT

In this study, waveform data obtained from Western Sichuan Seismic Array (WSSA) in China was utilized to reveal the temporal variations in coda attenuation around the eastern Tibet Plateau and Western Sichuan. Based on the single-scattering model, coda attenuation factor Q_c^{-1} is calculated in narrower overlapping frequency bands at 1.0–24 Hz by measuring the coda decay rates for local earthquakes before and after the Wenchuan mainshock. The temporal variations in coda attenuation are investigated within three periods. The period I lasted from January 2007 to the end of 2007. The period II lasted from January 2008 till Wenchuan earthquake. The period III lasted from the mainshock to the end of 2008. The resulted temporal variations demonstrate an increase in average Q_c^{-1} by approximately 35%–45% in the vicinity of Longmenshan and 30%–35% in Sichuan Basin after the Wenchuan earthquake in lower frequency bands within 1.25–8 Hz. On the contrary, the average Q_c^{-1} is shown to decrease by approximately 10%–18% in southern segment of Longmenshan, 15%–38% in the Chuan-Dian block, and 10–12% in the South China block. These results are confirmed by a statistical *t*-test at 99.9% confidence level. No statistically significant change in Q_c^{-1} (<10%) is found in the Songpan-Ganzi block after the mainshock. Temporal variations of coda attenuation differ significantly in individual blocks after the mainshock. The coda attenuation is proposed to be a beacon to tectonic static stress changes associated with the Wenchuan earthquake.

1. Introduction

The 12 May 2008 Wenchuan earthquake (M_W7.9) initiated on the southern Longmenshan thrust belt and struck west of Sichuan, China, along the eastern margin of Tibetan Plateau [1]. Coseismic slip initially occurring at about 10–20 km depth was estimated up to about 10 m [2]. The rupture propagated unilaterally northeastward on a northwest dipping fault for more than 320 km with the surface rupture length of 240 km. The dipping angle of the fault zone is estimated to be 70°–80° near the surface and 30°–60° near the hypocenter within the depth of 14–19 km [3]. The accompanying physical processes of earthquakes, such as coseismic stress changes, the migration of fluids and the formation of damage zones

* Corresponding author. State Key Laboratory of Simulation and Regulation of Water Cycle in River Basin, China Institute of Water Resources and Hydropower Research, A-1 Fuxing Road, Beijing 100038, China.
E-mail addresses: junhuahu_cas@163.com, 820602986@qq.com (J. Hu).
Peer review under responsibility of Institute of Seismology, China Earthquake Administration.
[1] Present/permanent address. China Institute of Water Resources and Hydropower Research, A-1 Fuxing Road, Beijing 100038, P. R. China.

Production and Hosting by Elsevier on behalf of KeAi

https://doi.org/10.1016/j.geog.2021.09.001

Please cite this article as: J. Hu, G. Zhang, L. Fu *et al.*, Temporal variations in coda attenuation associated with the 2008 Wenchuan (M_W7.9) Earthquake in SW, China, Geodesy and Geodynamics, https://doi.org/10.1016/j.geog.2021.09.001

in the shallow layers, can cause subtle changes in mechanical properties of nearby crustal material [4]. A broad region surrounding the source and the receiver is sampled many times by coda waves, which are intrinsically the multiple scattered S waves due to heterogeneities in the lithosphere [5]. Coda provides an elaborate means to monitor these subtle temporal changes.

Significant differences in the decay rate of coda have worldwide been observed between tectonically active and stable regions [6]. The quality factor of coda Q_C^{-1}, which is insensitive to source and receiver locations within the region, is generally introduced to describe the average attenuation of the crust. As a beacon to tectonic activity, high and low Q_c^{-1} indicate the active and stable regions, respectively. The frequency dependence of $Q_c^{-1}(\propto f^{-n}$, where f is the frequency and n is a constant) is proposed to be closely involved with tectonic activity. A strong frequency-dependent attenuation is contributed to the presence of highly fractured rocks, shallow high temperatures, hydrothermal activity and so on [7]. The variations of Q_c^{-1} imply the vertical and lateral inhomogeneities that could reflect important structural differences among seismic stations. The increase of Q_c^{-1} indicates an increase in the heterogeneities of the medium and vice versa. Temporal variations in Q_c^{-1} have also been widely investigated before and after large earthquakes. Significant increases have been observed before some large earthquakes [8]. For some events, an increase in Q_C^{-1} occurs after mainshock [9,10].

Q_c^{-1} was found to decrease after two earthquakes in Central Greece [11]. The first mainshock of magnitude $M_S = 5.0$ occurred on 25 May, 1992 at depth of 8.7 km and the second one of magnitude $M_S = 4.8$ on 11 November, 1992 at a depth of 7.3 km. Both events are located on a strike-slip fault towards NE coast of the Gulf of Patras. The attenuation of P waves Q_p^{-1} is estimated to decrease by about 20% associated with the first event and by about 15% for the second event. The clearly observed decrease of approximate 20% in P-wave attenuation is contradictory to the stress release if the attenuation is proposed to be relevant to crack closure. Therefore, the observed decrease in P-wave attenuation has been inferred to originate from variations in the state of saturation of rocks in the epicentral region. The results demonstrate the influence of fluid migration in the epicenter region on seismic wave attenuation.

However, no variation in Q_c^{-1} was found after the Loma Pieta California [12] and the Central Greece earthquake [13]. The October 18, 1989, Lama Prieta, California, earthquake ($M_W = 6.9$) occurred on California's Central Coast, approximately 16 km northeast of Santa Cruz on a section of the San Andreas Fault System. The oblique-slip rupture initialized at 10 km and below on a fault plane that dipped 70° to the southwest. Neither a preseismic nor a postseismic change in coda Q was found at the level of about 5% over the frequency range 2–15 Hz. Even no coseismic change at the same threshold was detected despite the occurrence of a major earthquake. The observed slight variations are neither spatially coherent nor correlated between frequency bands. The mainshock of June 15,1995, Egion, Central Greece earthquake ($M_S = 6.2$) occurred at a depth of 12.8 km. The selected events are confined within a cubic volume approximately 30 km on each side with the magnitude range of $2.5 < M_L < 3.0$. No significant variation in the overall means of Q_c was found prior to ($Q_{f\ =\ 4\ Hz} = 183$, $Q_{f\ =\ 8\ Hz} = 266$) and after ($Q_{f\ =\ 4\ Hz} = 184$, $Q_{f\ =\ 8\ Hz} = 273$) the mainshock.

Those observed variations in Q_C^{-1} are argued to shed light on subtle changes in attenuation and/or scattering properties of heterogeneous crust. The underlying physical mechanisms probable include coseismic crack opening or post-seismic relaxation processes, such as fluid migration into cracks, crack healing, and rock compaction caused by the major earthquakes [14,15]. In addition, net volume increase due to cracks opening in the rocks and/or aseismic creep activities is proposed to increase the crack density and hence coda attenuation in the region [16]. An inhomogeneous distribution of crack clusters has been expected in a vast region compared with the aftershock region. The gradual appearance of such crack clusters seems to be the most plausible mechanism for large value of Q_C^{-1} during the stress accumulation stage.

This study focuses on the temporal variations of coda attenuation in the crust associated with the Wenchuan earthquake at the regional scale. The abundant waveforms recorded by the Western Sichuan Seismic Array (WSSA) from January 2007 to December 2008 are preprocessed in appropriated methods to determine the time window of coda waves for further analysis. Under the assumption of single-scattering model, coda attenuation factor is derived within narrower overlapping frequency bands of 1.0–24 Hz for the local earthquakes occurring before and after Wenchuan mainshock. Next, the temporal variations in coda attenuation are investigated in details within three-time intervals. The first interval I lasted from January 2007 to December 2007; the second interval II lasted from January 2008 till the Wenchuan earthquake; the final interval III lasted from the mainshock to December 2008. The results demonstrate that significant differences in temporal variations of coda attenuation are found within individual blocks. To verify the resulted temporal variations in average coda attenuation, statistical t-tests are conducted at 99.5% confidence level. It indicates that Q_C^{-1} variations can be a beacon to the change of static tectonic stress associated with the Wenchuan earthquake.

2. Data and method

2.1. Data

The Western Sichuan Seismic Array (WSSA), which was deployed in western Sichuan in October 2006 well prior to the Wenchuan earthquake, consists of 309 portable broadband digital seismic stations. WSSA remained functional for over two years till December 2009 and monitored approximately 2/3 proportion of the activated fault system associated with the Wenchuan earthquake. Therefore, the network provides much waveform data recorded before, during and post the mainshock. The data obtained from WSSA has been utilized to reveal the genesis and process of the Wenchuan earthquake and the seismic structure of Eastern Tibetan Plateau and Longmenshan belt [17,18]. A waveform matched-filter technique was employed to determine the evolution and distribution of early aftershocks following the Wenchuan Earthquake, which imposes additional conditions on the plateau uplifting mechanism [19]. Temporal seismic velocity changes were tracked at a regional scale by applying a doublet analysis on continuous recordings of codas of seismic noise cross-correlation functions [20]. It was found that seismic velocity decrease of 0.08% occurs in the fault region post seismic with pre-seismic fluctuations within 0.02%. It was also revealed that the spatial velocity variations are consistent with the volumetric strain change, indicating the irrelevance of the sediments to the seismic response.

Fig. 1(a) presents the main geological blocks (red dash lines) and the station locations (blue triangles) within the study area. According to the main active boundaries, the study area is divided into several blocks, including Sichuan Basin (SB), Songpan-Ganzi (SG), Chuan-Dian (CD), South China (SC), Western Yunnan (WYN), Southern Yunnan (SYN), fault zones of Longmenshan (LMS), Xianshuihe(XSH), Anninghe (ANH), Xiaojianghe (XJH), and Zemuhe (ZMH) [21]. The study area resides within 26°–32°N and 99.5°-105°E, covering the gross range of WSSA. The locations of 309 stations are represented by the blue triangles with average station

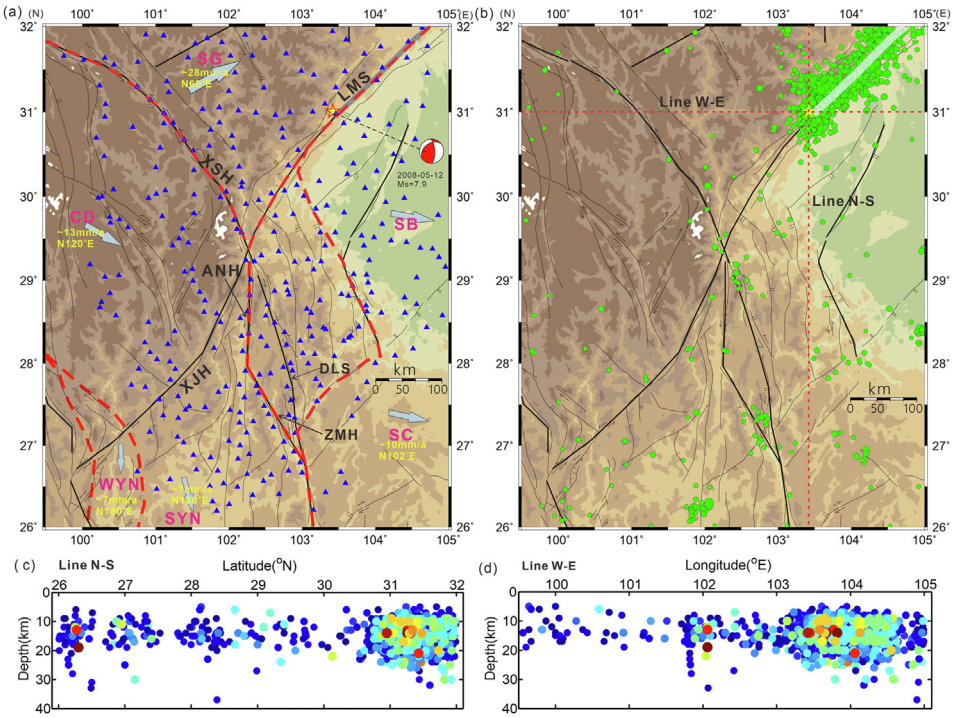

Fig. 1. (a) The location of stations (blue triangles) and the block boundaries (red dash lines). The thick black lines represent the mapped faults and the thin black lines represent faults active in the past 10 Ky [19]. The gray arrows show the direction of relative movements for individual block. The star and the beach ball indicate the epicenter and focal mechanism of the Wenchuan earthquake, respectively. Bold black lines demonstrate major faults in the studying region. SB, SG, CD, SC, WYN,SYN, LMS, XSH, XJH, ANH and ZMH stand for Sichuan Basin, Songpan-Ganzi block, Chuan-Dian block, South China, Western Yunnan, Southern Yunnan, Longmenshan, Xianshuihe, Xiaojianghe, Anninghe and Zemuhe, respectively. (b) The spatial distribution of selected events (green circles) with magnitude of $3.0 \leq M_S \leq 6.5$ recorded from January 01, 2007 to December 31, 2008 in the study region. The bold light gray line indicates the projected main rupture plane of the Wenchuan earthquake. (c) and (d) show the vertical profiles of selected events projected along the Line N–S and Line W–E (red dash lines in (b)), respectively. The magnitude of event is proportional to the color ranging from blue to red. The lighter color indicates the larger magnitude.

spacing of 20–30 km, and the closest one locates approximately 20 km to the epicenter. Each station is equipped with three-component accelerometers of Type CMG-3ESPC with flat responses to the velocity of ground motion within 0.05–20 Hz. Waveform data are recorded at various sampling rates through linear-phase FIR filters using a 24-bit analog-to-digital converter of Type REFTEK-130B. The waveforms are extracted in continuous mode by 40 samples per second for each signal channel. The seismic recordings are synchronized by GPS receivers. Vertical components with a high signal-noise ratio are employed in our study. Fig. 1(b) shows the spatial distribution of selected 931 events (green circles) with the magnitude of $3.0 \leq M_S \leq 6.5$ recorded from January 01, 2007 to December 31, 2008. The vertical profiles of selected events projected along the Line N–S and Line W–E are demonstrated in Fig. 1(c) and (d), respectively. The histograms of the number of events with magnitude and depth are presented in Fig. 2. To relief the effects of aftershocks and bias associated with source distribution, the events locating in 30-32° N and 103-105° E (the rectangle) from May 12 to June 12 are excluded from the calculation of average Q_C^{-1}. The histogram only shows the events that has been included in the calculation. Details can be referred to Fig. 3. The focal depths of the analyzed events range within H = 0–35 km. The hypocentral distance between the selected station and event pair is set to be D = 20–200 km.

2.2. Method

The isotropic single-scattering model is employed due to its flexibility in the analysis time-window selection [22]. Instant coda analysis can be conducted excessing the S-wave arrival [23]. For a bandpass filtered seismogram centered at the frequency of f, the ratio of the mean energy density of the scattered waves to the primary S-wave energy can be approximated by the square of the amplitude ratio as

$$F(t) = \log\left[\left(\frac{A_c(t)}{A_s}\right)^2 K^{-1}(\alpha)\right] = C(f) - b(t - t_s) \quad (1)$$

$$b = 2\pi f[\log(e)] / Q_c \quad (2)$$

where A_s indicates the maximum amplitude of S wave. $A_c(t)$ represents the mean amplitude of the coda around the lapse time t measured from the origin time of earthquake. The lapse time of S wave is indicated with t_s. The source factor $C(f)$ for certain f is assumed to be constant. The time-dependent spreading factor $K(\alpha)$ can be given as $K(\alpha) = (1/\alpha)\ \ln\ [(\alpha\text{-}1)/(\alpha+1)]$, where $\alpha = t/t_s$. The quality factor of the seismic coda Q_c can be easily obtained from the slope of linear equation, b, by the least-square method. Since the proposed model is only applicable for a single frequency, an octave-width bandpass filter is generally applied to the raw waveform to calculate the coda attenuation [24]. Extreme narrow bandwidth will cause high oscillation of filtered coda envelope, thus difficulty in stable estimation of Q_C^{-1}. To avoid numerical singularities, baseline correction and cosine taper with a width of 10% of the full-time length are performed on both ends of waveform [25]. Then, a phaseless four-pole Butterworth bandpass filter is applied to the waveform at frequency of $f_0 = 1.25, 1.75, 2.5, 3.5, 5, 8, 12, 16, 20$, and 24 Hz with breadth of two-thirds of the center frequency. Root-Mean-Square (RMS) amplitudes (A_{rms}) are calculated from 2s

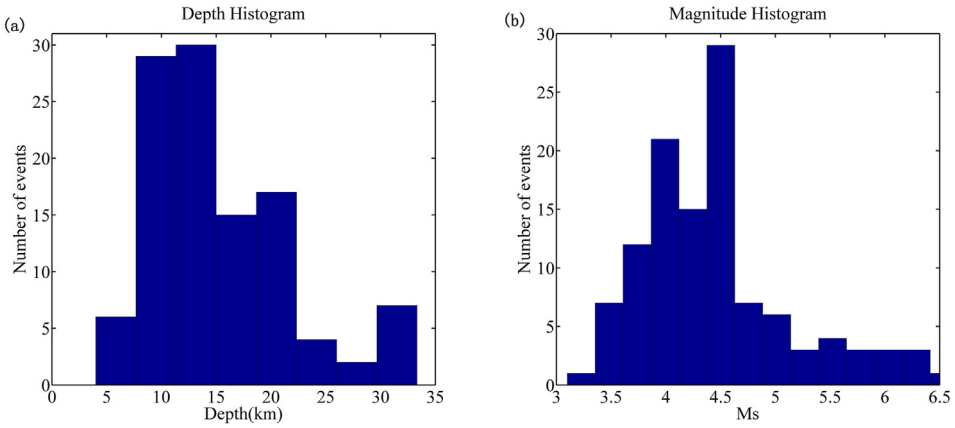

Fig. 2. The number of events with (a)- depth and (b)- magnitude recorded from January 01, 2007 to December 31, 2008 in the study region. To relief the effects of aftershocks and bias associated with source distribution, the events locating in 30-32° N and 103-105° E (the rectangle) from May 12 to June 12 are excluded from the calculation of average Q_C^{-1}. The histogram only shows the events that have been included in the calculation.

time-window with increment of 0.4 s. The RMS amplitude is assigned to the time-window center. Assuming the recorded waveform is a linear superposition of noise and signal, corrected RMS amplitude can be derived from $A_c = (A_{2T}\text{-}A_{2N})^{1/2}$, where A_T and A_N indicate the RMS amplitude of the seismic trace and the noise before P wave arrival, respectively [23]. The starting time of window is set to be 1−2 s excessing S wave arrival for the decay stability. The linear fitting range of $F(t)$ is generally determined by the major turning point of the $F(t)$ data points on the signal filtered around the center frequency f. The window-moving process stops if $A_T/A_N < 2$. The fitting error is given by

$$\delta b = ss/t_w \tag{3}$$

where ss and t_w indicate the square root error between recorded $F(t)$ and the fitting time-window length, respectively. The corresponding error for Q_c can be given

$$\sigma = 2\pi f[\log(e)]\delta b \Big/ \left(b^2 - \delta b^2\right) \tag{4}$$

A stable estimation is obtained by simultaneously searching the optimal decay rate fitting all waveforms [16]. Around individual station, the average Q_c at single frequency for all associated events can be calculated by

$$< Q_c > = \left[\sum\left(Q_{ci} \Big/ \sigma_i^2\right)\right] \Big/ \left[\sum\left(1 \Big/ \sigma_i^2\right)\right] \tag{5}$$

Summation is operated over all Q_{ci} with standard deviations σ_i<15%. With the weight being the inverse of its variance, better values contribute more to $< Q_c >$ and worse less. The variance of $< Q_c >$ is given by

$$\sigma_m^2 = \left[\left(1 \Big/ \sigma_i^2\right)\sum(Q_{ci} - < Q_c >)^2\right] \Big/ \left[(n-1)\sum\left(1 \Big/ \sigma_i^2\right)\right] \tag{6}$$

Fig. 4 demonstrates a data processing example for the vertical waveform recorded at station KYA19 for a M_S4.3 earthquake which occurred to southwest of the station with epicentral distance of 63.5 km and depth of 11 km approximately. The coda window is set to be T_w = 15−35 s starting from 1.2 times S-wave arrival ($t > 1.2t_s$). Such setting is reasonable because multiple scattering waves dominating for lapse time longer than S-wave mean free time would lead to apparent low estimation of Q_c^{-1} [26]. Consequently, the frequency-dependent power-law form of $Q_c^{-1}(f) = Q_0 f^{-n}$ in f = 1.0−24 Hz for each station can be obtained.

3. Selection of events and stations

Temporal variations in Q_C^{-1} are investigated pre- and post-seismic during three-time intervals. The first time interval I lasted from January 2007 to December 2007; the second one II lasted from January 2008 till May 12, 2008, when the Wenchuan mainshock struck. The third one III lasted from the mainshock to December 2008. The events occurring since January 2007 are chosen for explicitly extracting the pre-seismic variations in coda attenuation. The time interval is selected in order to exclude the effects of other earthquakes with magnitude M_S > 6.5 on the Wenchuan earthquake. Such time interval is adequate for detecting possible Q_C^{-1} variations preceding Wenchuan mainshock. Prior to analysis on any possible temporal variations in coda attenuation, the space-time distribution pattern of events utilized in our study has been plotted to inspect the influence of spatial changes of event locations on these variations (Fig. 3). It can be seen that the epicenters distribute almost uniformly during periods I and II before the mainshock. However, a clear cluster indicated by the black solid rectangle concentrates around the source region after the occurrence of Wenchuan earthquake. To relief the effects of aftershocks and bias associated with source distribution, the events locating in 30-32° N and 103-105°E (the rectangle) from May 12 to June 12 are excluded from the calculation of average Q_C^{-1}.

Several stations with high-quality waveform data are selected and divided into eight networks (Fig. 5). The network LMS around the rupture segment of Longmenshan consists of stations KMX01-KMX03, KMY01-KMY09, and KWC01-KWC05. The network SLMS located on the unruptured southern segment of Longmenshan consists of stations KYA01-KYA19; the network SB located on Sichuan basin consists of stations KCD01-KCD11; the network SG located in Songpan-Ganzi block consists of stations KDB01-KDB07, KXJ01-KXJ05, and KJC01-KJC05, the network XSH located in the Xianshuihe fault zone consists of stations KDF01-KDF09, the network CD located in Chuan Dian block consists of stations KYJ01-KYJ06. The network XJH near the Xiaojianghe fault zone consists of stations XMN01-XMN06. The network SC located in South China block consists of stations KLS01-KLS18. In the following, the temporal variations in Q_C^{-1} during three-time intervals I-III are investigated in details.

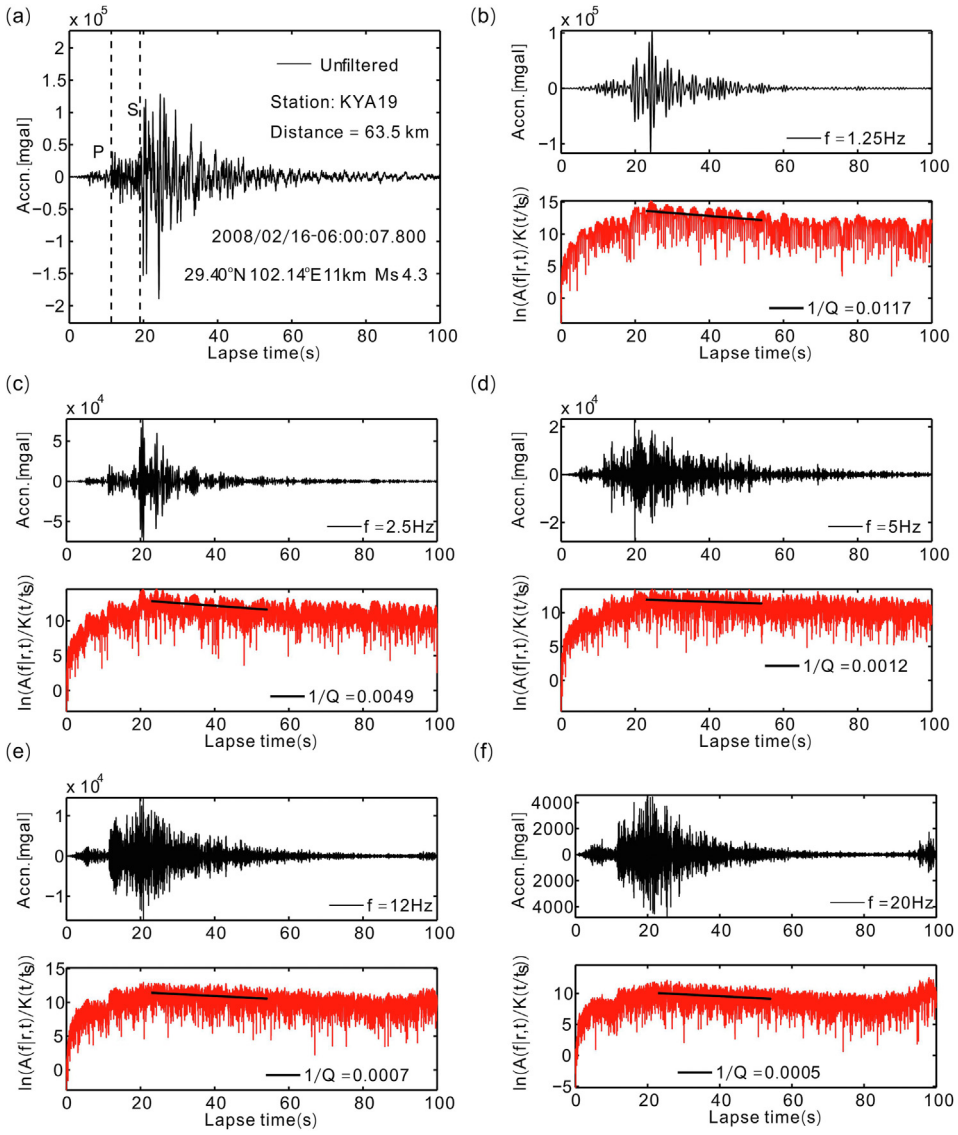

Fig. 4. Procedure for determining Q_C^{-1} values when applied to the selected one event ($M_S = 4.3$) recorded at station KYA19 with epicentral distance of 63.5 km and depth of 11 km approximately. (a) shows the unfiltered vertical component seismogram with sampling of 100 Hz. The source parameters of the event are shown on the lower right. (b), (c), (d), (e) and (f) are the bandpass filtered seismograms with central frequencies $f_0 = 1.25$, 2.5, 5, 12 and 20 Hz, respectively. The filtered waveforms and their corresponding logarithmic Root-Mean-Square envelopes are shown on the top and bottom panels in each subplot, respectively. The slope of regression fit to envelopes expressed by a small line over $T_w = 35$ s coda window at 1.2 t is used to estimate Q_C^{-1}. The values of Q_C^{-1} are also given in each subplot for each frequency band.

4. Results

The temporal average Q_C^{-1} at networks LMS, SLMS, SG, XSH, CD, XJH, SC, and SB, are presented in Figs. 6–13 for three-time intervals (I-III) within $f = 1.0$–24 Hz, respectively. By comparing the average Q_C^{-1} for each time interval with that for the preceding time interval, the relative temporal variations in Q_C^{-1} at all frequencies of1.0–24 Hz for the eight station networks are summarized in Fig. 14. The Students *t*-test is performed to verify the significance of temporal variations. In our case, the null hypothesis indicates the equivalence in the means of Q_C^{-1} between the two-time intervals with the significance level for null hypothesis rejection less than 5%. The solid and dash line segments represent the temporal variations of average Q_C^{-1} statistically significant with confidence level no less than 95% and those statistically insignificant with confidence less than 95%, respectively. The significance levels based on the *t*-test for individual periods of all frequency bands are summarized in Tables A.1–A.8 in the section of Appendices.

For the network LMS locating in the rupture zone of Wenchuan earthquake (Fig. 6), the average Q_C^{-1} slightly increases less than 20% at lower frequencies of 1.25, 1.75, 2.5, 3.5, and 5 Hz during interval II. Almost no temporal variation is observed at higher frequencies of 16, 20, and 24 Hz. The variations are not statistically significant at a high level. On the contrary, the average Q_C^{-1} increases up to approximately 35%–45% at all frequencies of 1.25–24 Hz during interval III. Based on the one-sided Students *t*-test, post-seismic variations within one standard deviation of mean Q_C^{-1} are statistically significant at 95% confidence level. Similar results are found in the network SB in the vicinity of main rupture zone (Fig. 7). Increase in the average Q_C^{-1} has been no more than 10% during intervals I-II while up to approximately 30%–35% during intervals II-III. These post-seismic increases are significant at confidence level

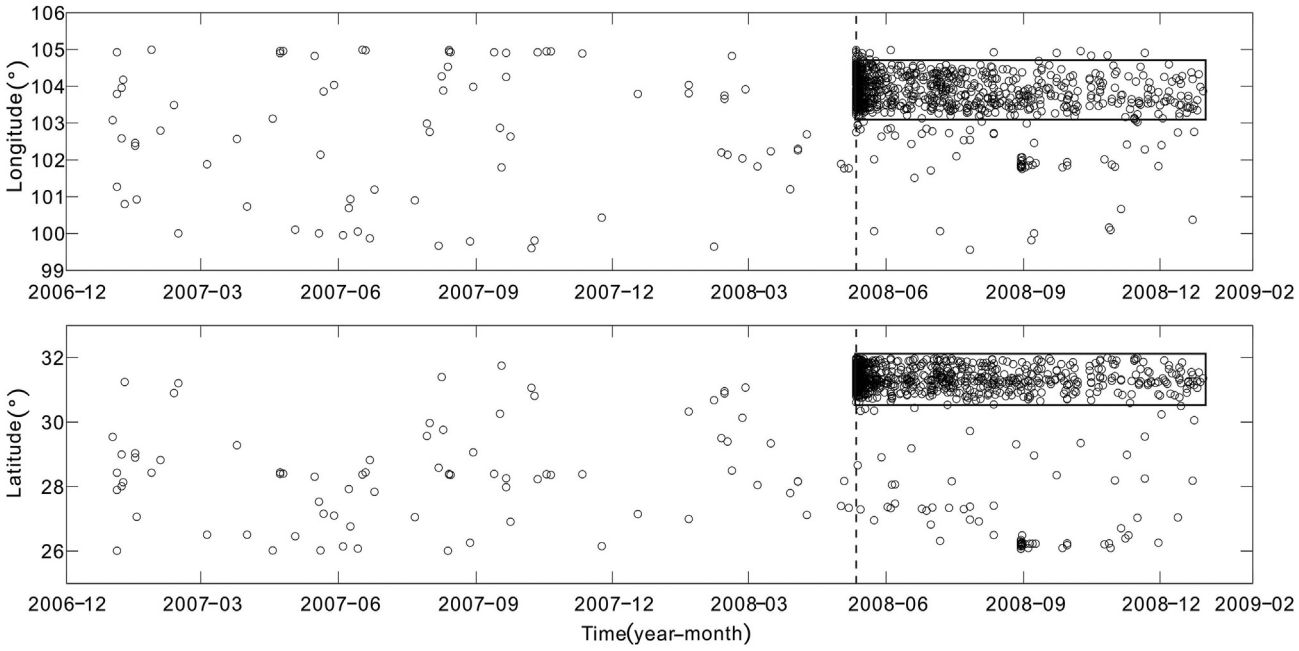

Fig. 3. Space–time plots of the selected earthquakes during the study period (January 2007 to December 2008). The vertical dash line indicates the time of occurrence of the mainshock of the 2008 Wenchuan earthquake. The rectangle represents the cluster associated with the 2008 Wenchuan earthquake (M_S 7.9). To relief the effects of aftershocks and bias associated with source distribution, the events locating in 30-32° N and 103-105° E (the rectangle) from May 12 to June 12 are excluded from the calculation of average Q_C^{-1}.

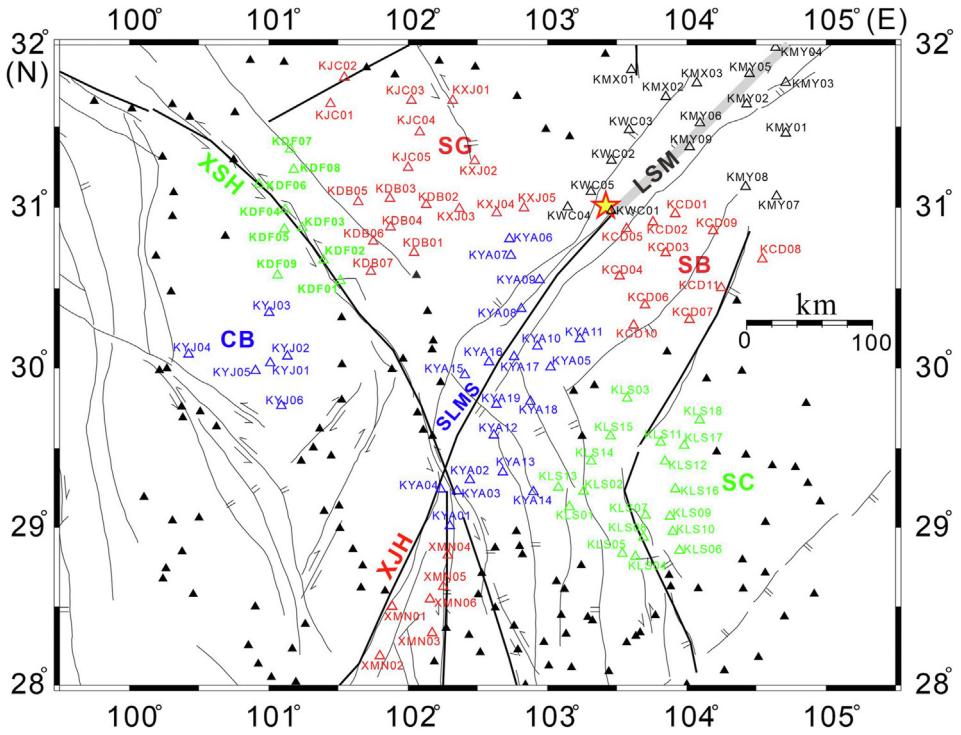

Fig. 5. The selected eight station networks with high quality waveform to show the temporal variations in Q_C^{-1} for individual blocks. These station networks are indicated with various colors. SB, SG, CD, SC, LMS, XSH and XJH stand for Sichuan Basin, Songpan-Ganzi, Chuan-Dian,South China, Longmenshan, Xianshuihe, and Xiaojianghe, respectively. SLMS is short for the southern segment of the Longmenshan fault zone. The star indicates the epicenter of the mainshock of Wenchuan earthquake. The thick gray line indicates the rupture segment along the Longmenshan fault zone. The thick and thin black lines indicate the mapped faults and the faults active in the past 10 Ky. The filled black triangles indicate the stations in the Western Sichuan Seismic Array (WSSA).

of 95%, indicating a close relation to Wenchuan earthquake. The larger standard deviation of Q_C^{-1} for SB indicates more dramatic tectonic stress change in this region.

For the network SLMS (Fig. 8), no statistically significant post-seismic variation is found in the average Q_C^{-1} during intervals II-III at frequencies of 1.25–8 Hz. It can be probably inferred that

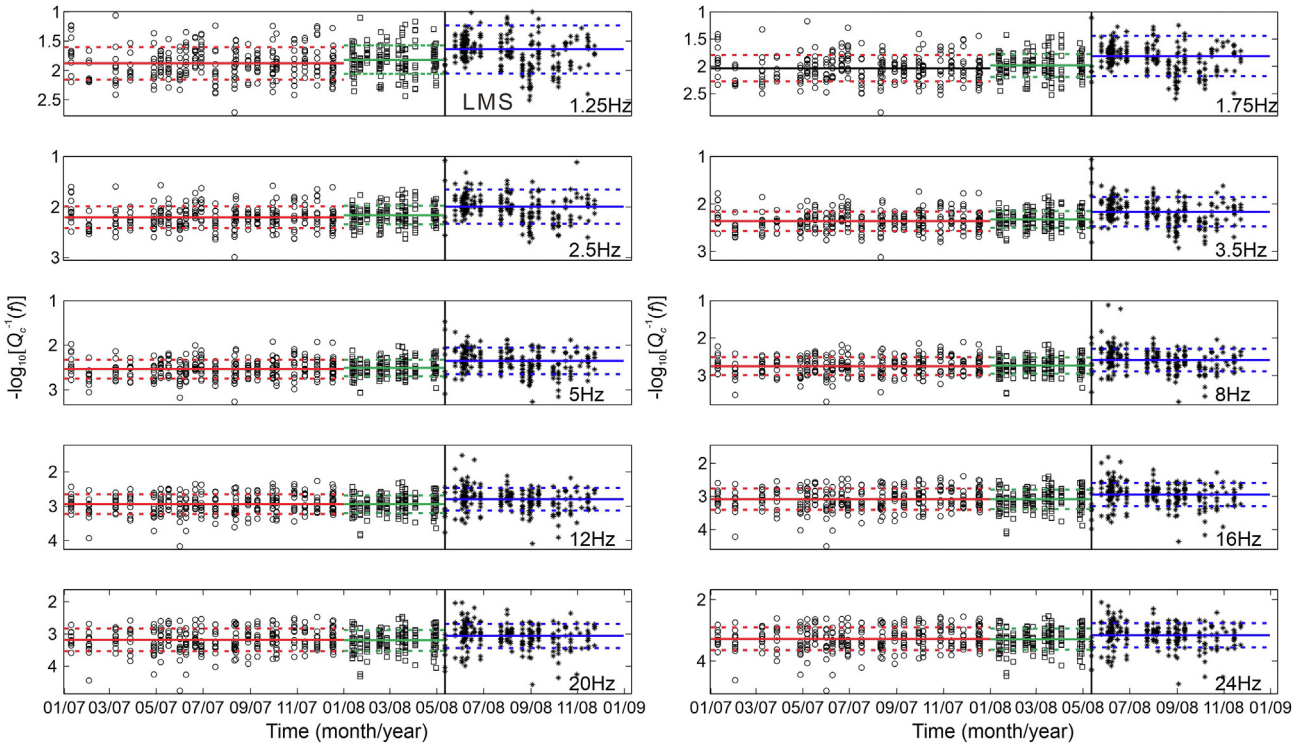

Fig. 6. Temporal variations in Q_C^{-1} within three time intervals (I-III) at frequencies of $f = 1.0–24$ Hz for the selected station network LMS shown in Fig. 5. The results for I, II, and III are indicated with red, green, and blue lines, respectively. The solid line shows the average over each time interval bounded by the dashed lines indicating the standard deviation. Different symbols are used to show the data points for different time intervals. The vertical lines indicate the occurrence time of the mainshock of the Wenchuan earthquake.

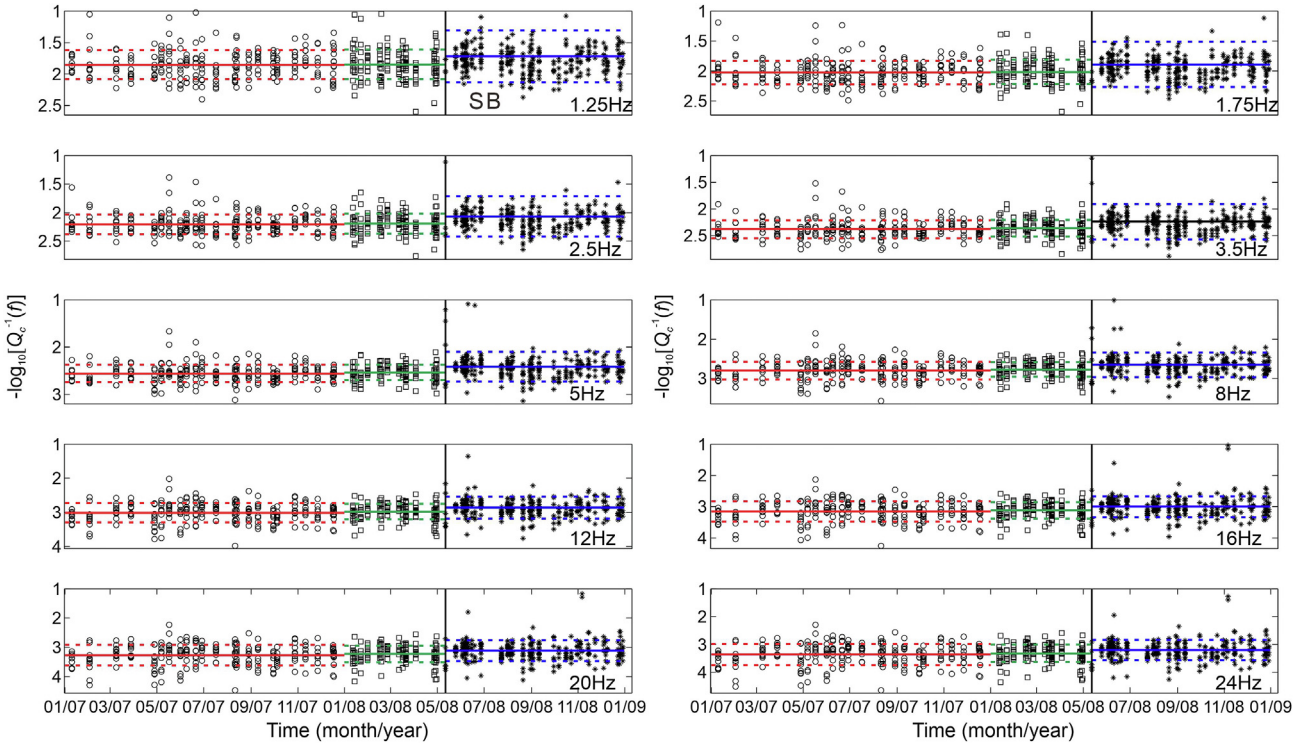

Fig. 7. Temporal variations in Q_C^{-1} within three time intervals (I-III) at frequencies of $f = 1.0–24$ Hz for the selected station network SB shown in Fig. 5. The results for I, II, and III are indicated with red, green, and blue lines, respectively. The solid line shows the average over each time interval bounded by the dashed lines indicating the standard deviation. Different symbols are used to show the data points for different time intervals. The vertical lines indicate the occurrence time of the mainshock of Wenchuan earthquake.

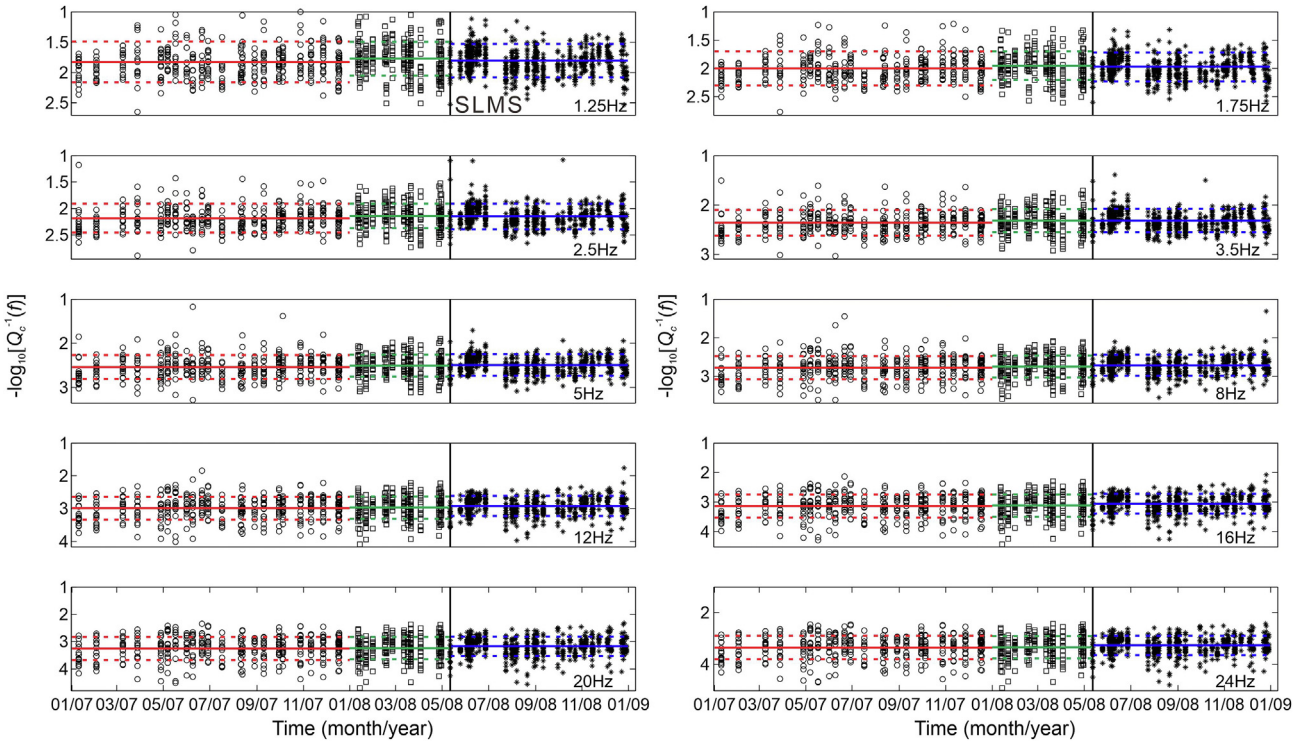

Fig. 8. Temporal variations in Q_C^{-1} within three time intervals (I-III) at frequencies of $f = 1.0–24$ Hz for the selected station network SLMS shown in Fig. 5. The results for I, II, and III are indicated with red, green, and blue lines, respectively. The solid line shows the average over each time interval bounded by the dashed lines indicating the standard deviation. Different symbols are used to show the data points for different time intervals. The vertical lines indicate the occurrence time of the mainshock of Wenchuan earthquake.

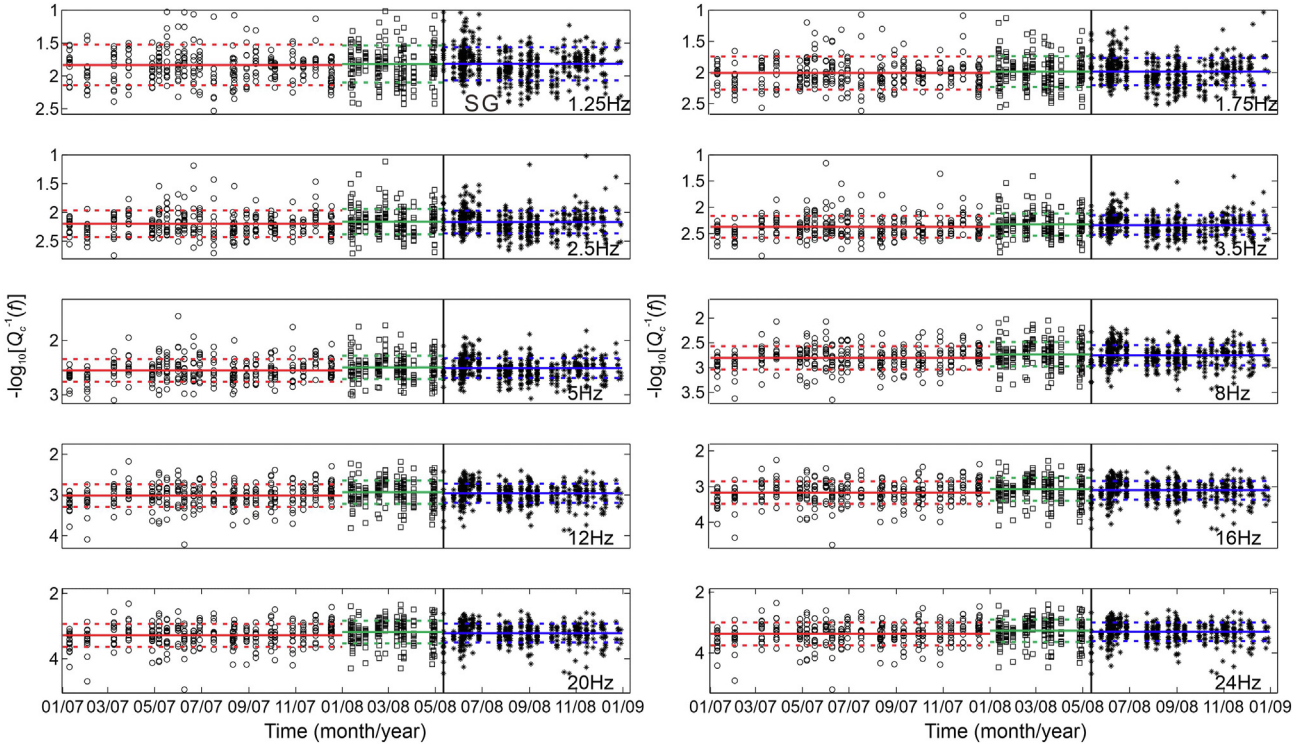

Fig. 9. Temporal variations in Q_C^{-1} within three time intervals (I-III) at frequencies of $f = 1.0–24$ Hz for the selected station network SG shown in Fig. 5. The results for I, II, and III are indicated with red, green, and blue lines, respectively. The solid line shows the average over each time interval bounded by the dashed lines indicating the standard deviation. Different symbols are used to show the data points for different time intervals. The vertical lines indicate the occurrence time of the mainshock of Wenchuan earthquake.

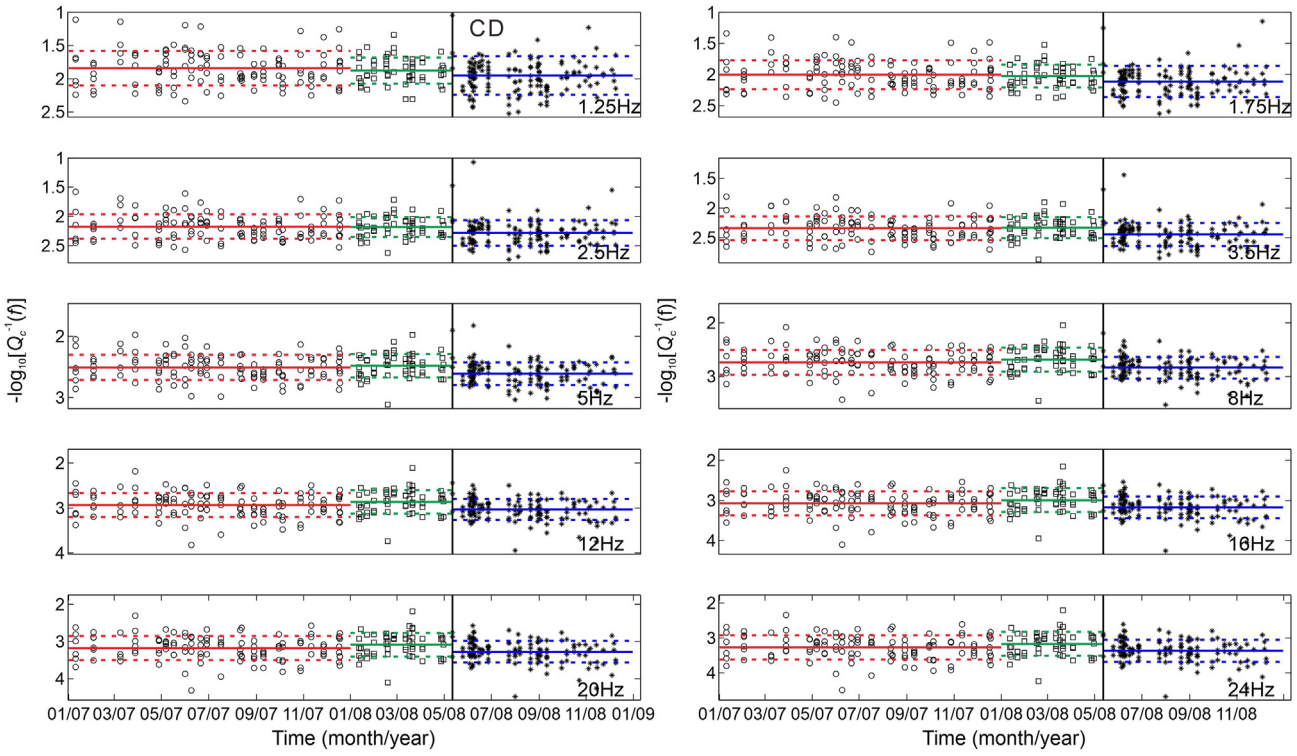

Fig. 10. Temporal variations in Q_C^{-1} within three time intervals (I-III) at frequencies of $f = 1.0-24$ Hz for the selected station network CD shown in Fig. 5. The results for I, II, and III are indicated with red, green, and blue lines, respectively. The solid line shows the average over each time interval bounded by the dashed lines indicating the standard deviation. Different symbols are used to show the data points for different time intervals. The vertical lines indicate the occurrence time of the mainshock of Wenchuan earthquake.

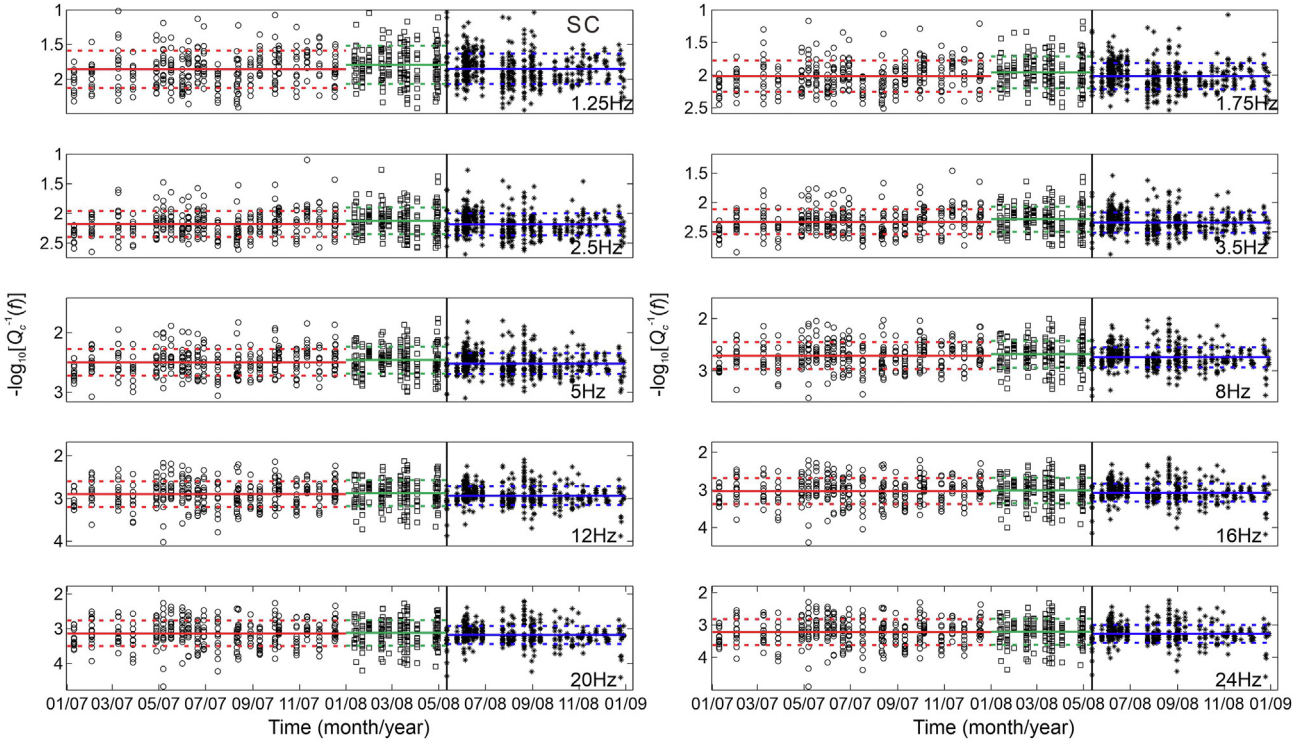

Fig. 11. Temporal variations in Q_C^{-1} within three time intervals (I-III) at frequencies of $f = 1.0-24$ Hz for the selected station network SC shown in Fig. 5. The results for I, II, and III are indicated with red, green, and blue lines, respectively. The solid line shows the average over each time interval bounded by the dashed lines indicating the standard deviation. Different symbols are used to show the data points for different time intervals. The vertical lines indicate the occurrence time of the mainshock of Wenchuan earthquake.

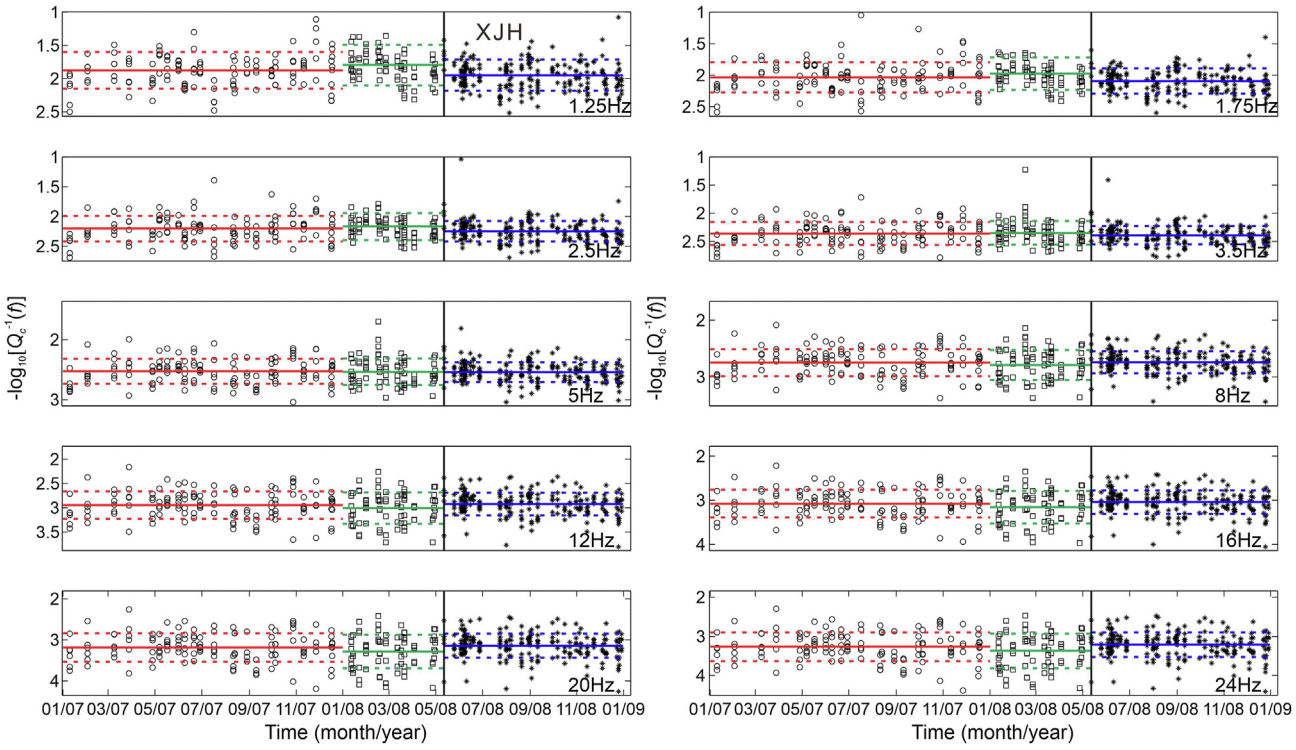

Fig. 12. Temporal variations in Q_C^{-1} within three time intervals (I-III) at frequencies of $f = 1.0–24$ Hz for the selected station network XJH shown in Fig. 5. The results for I, II, and III are indicated with red, green, and blue lines, respectively. The solid line shows the average over each time interval bounded by the dashed lines indicating the standard deviation. Different symbols are used to show the data points for different time intervals. The vertical lines indicate the occurrence time of the mainshock of Wenchuan earthquake.

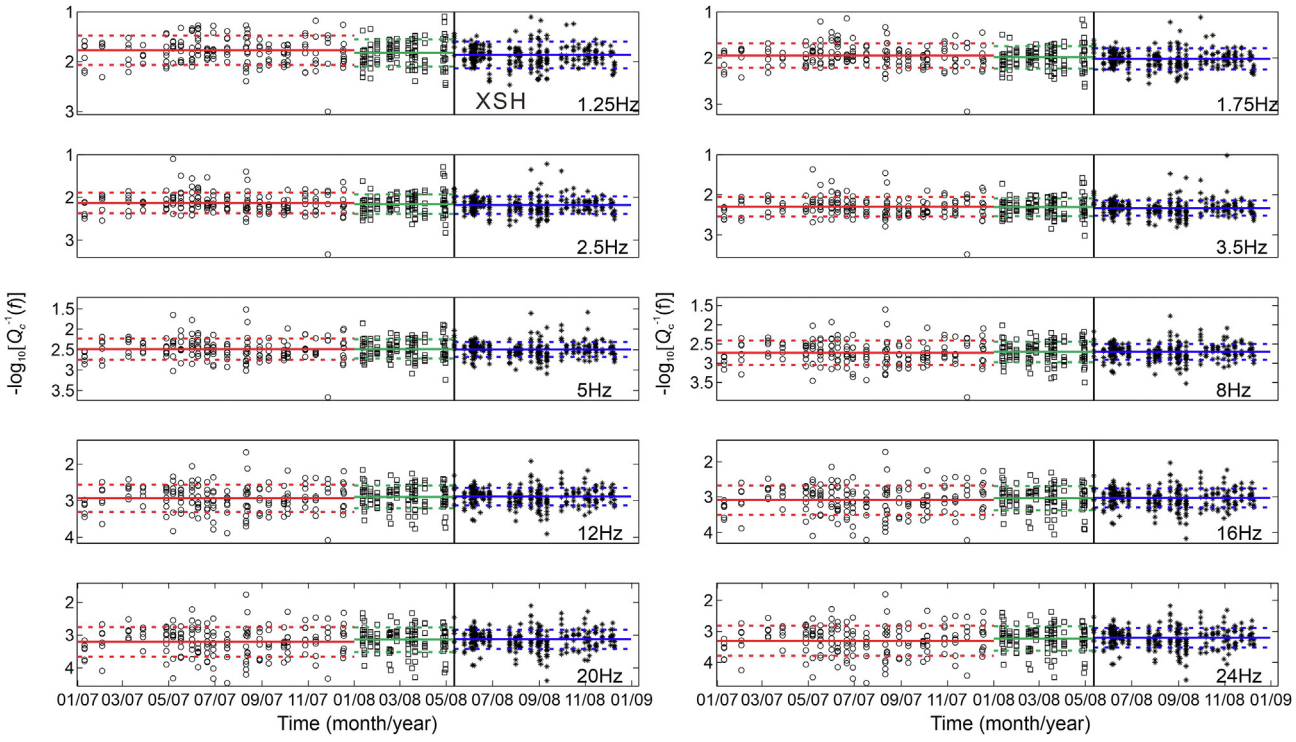

Fig. 13. Temporal variations in Q_C^{-1} within three time intervals (I-III) at frequencies of $f = 1.0–24$ Hz for the selected station network XSH shown in Fig. 5. The results for I, II, and III are indicated with red, green, and blue lines, respectively. The solid line shows the average over each time interval bounded by the dashed lines indicating the standard deviation. Different symbols are used to show the data points for different time intervals. The vertical lines indicate the occurrence time of the mainshock of Wenchuan earthquake.

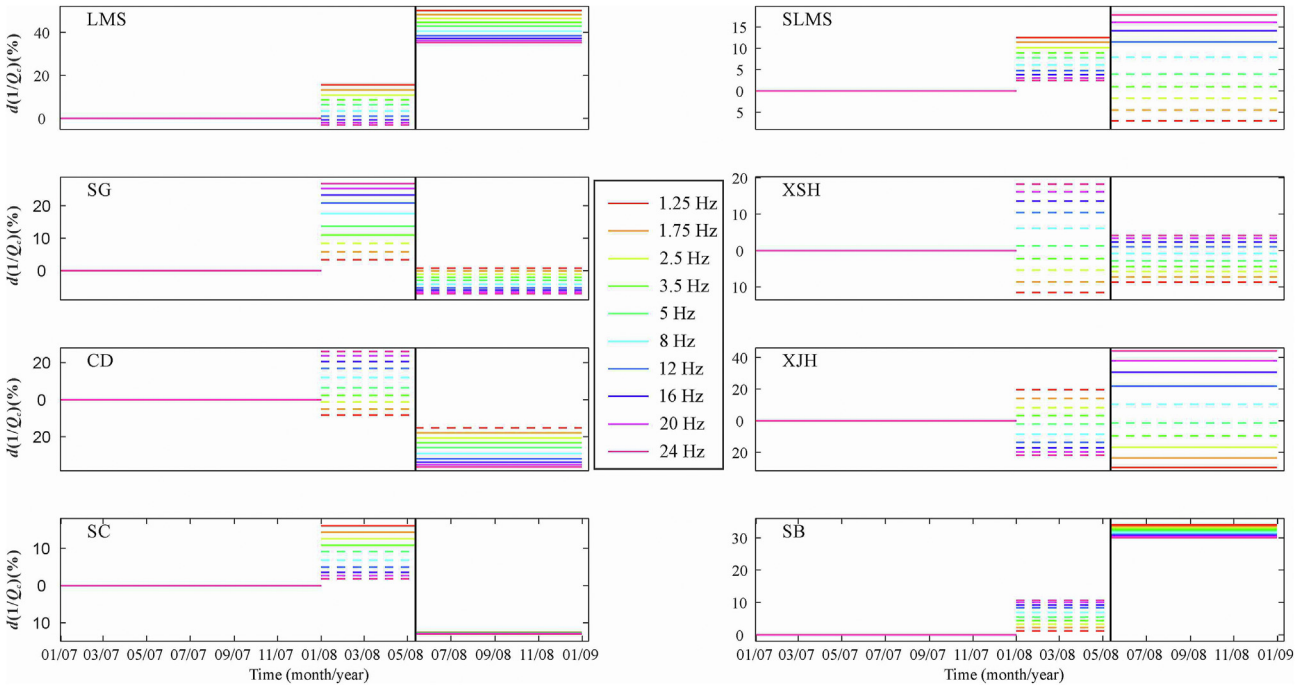

Fig. 14. The relative temporal variations in Q_C^{-1} at all frequencies of 1.0–24 Hz for the eight station networks. It can be seen that the temporal variations in Q_C^{-1} as statistical changes at all the frequencies f = 1.0–24 Hz differ significantly for the selected station networks in individual blocks. The vertical lines indicate the occurrence of the mainshock of the Wenchuan earthquake. The solid and dash line segments represent the temporal variations of average Q_C^{-1} statistically significant with confidence level no less than 95% and those statistically insignificant with confidence less than 95%, respectively. It is noticeable that a statistically significant increase in Q_C^{-1} from II to III is observed for LMS locating in the rupture zone of the mainshock.

the structure beneath southern segment of Longmenshan has remained relatively intact without significant change in coda attention throughout the process of the Wenchuan earthquake. It is observed that the average Q_C^{-1} has increased by approximately 10–12% at frequencies of 1.25–2.5 Hz during I-II and 10%–18% at frequencies of 12–24 Hz during II-III. For the network SG (Fig. 9), despite no statistically significant change post the mainshock, there is an evident increase of approximately 10%–30% in the average Q_C^{-1} at higher frequencies of 5–24 Hz during pre-seismic intervals I-II. It is probably involved with the stress accumulation in the Songpan-Ganzi block before the occurrence of the Wenchuan earthquake due to the continuous pushing effect of block movements.

Statistically significant decreases in the average Q_C^{-1} reach approximately up to 15%–38% and 12% at all frequencies of 1.0–24 Hz for networks CD and SC, respectively (Figs. 10 and 11). It suggests that the strain relaxation induced by the Wenchuan earthquake has promoted these two blocks to be rigid and stable. No statistical change is observed during interval II in CD. It is also noted that the average Q_C^{-1} in SC has gained a statistically slight increase of 10%–18% during interval II at lower frequencies of 1.25–3.5 Hz, indicating the subtle tectonic stress change in South China block prior to the mainshock.

For the network XJH (Fig. 12), the averaged Q_C^{-1} has slightly increased during interval II preseismic but significantly decreased during interval III at 1.25 and 1.75 Hz. On the contrary, Q_C^{-1} has slightly decreased during interval II preseismic but significantly increased during interval III at frequencies of 8–20Hz. Despite variations in Q_C^{-1} being 20% preseismic and 10% postseismic, such change proves to be statistically insignificant compared with the background level according to the t-test (indicated with dash lines). For the network XSH (Fig. 13), during intervals I-II a slight decrease in Q_C^{-1} is observed at lower frequencies of 1.25 and 1.75 Hz without statistically significant variation at other frequencies. On the contrary, during intervals II-III, the average Q_C^{-1} has dramatically increased by 25–45% at higher frequencies of 12,16, 20, and 24 Hz while moderately decreased by 10%–30% at lower frequencies of 1.25,1.75, and 2.5Hz. It probably implies the depth variations of static tectonic stress in the crust of XJH associated with the Wenchuan earthquake.

5. Analysis and discussion

It is noticeable that there exists a significant high Q_C^{-1} located in the epicenter of the Wenchuan earthquake (Fig. 14). It is in good agreement with the S-wave velocity (V_s) and Poisson's ratio (σ) structure obtained from inverting travel times of the aftershocks and other local events around the LMS fault zone [27]. Their results show that the structure of the LMS fault zone north of the Wenchuan mainshock differs significantly from that south of the mainshock. The southern segment of LMS with low-V_s and high-σ anomalies corresponds to the high Q_c^{-1} in the southern segment, suggesting lower medium strength or absence of strong asperities there, where the elastic energy is not easy to accumulate.

Low velocity generally indicates the pores expanding, the cracks opening, or the medium softening, which will lead to increase in coda attenuation. The regions in the LMS fault belt and the SB block are proposed to undergo significant coseismic velocity decrease by approximately 0.08% [20]. These results are consistent with significant increase of the average Q_c^{-1} in LMS and SB regions in our results (Fig. 14). In addition, almost no crustal velocity change in the southern LMS confirms the statistically insignificant post-seismic variation at SLMS. However, the similar velocity decreases occurring on both sides of Longmenshan fault contradicts the evident

difference in Q_C^{-1} variations between SG and SB blocks. Our results prove more reasonable due to significantly different geological characteristics between Sichuan basin and Songpan-Ganzi block.

A strong frequency-dependent attenuation is expected to play an essential role in areas where the presence of highly fractured rocks, shallow high temperatures, and hydrothermal activity could influence the frequency content of the seismic signals. The results of Figs. 6–13 show that, in general, the Q_c^{-1} is high in active regions in all frequency ranges as compared to the stable regions, indicating that the entire lithosphere beneath active regions is relatively more attenuative than that of the stable regions. The results of Figs. 6–13 also show that Q_c^{-1} decreases with frequency. The frequency–dependence relationship indicates that attenuation at higher frequencies is less pronounced than at lower frequency. The influence of the attenuation of the medium decreases with increase in frequency. The high Q_c^{-1} values at lower frequency range (1–3 Hz) can be attributed to the energy loss due to numerous heterogeneities. The estimated low Q_c^{-1} values at greater than 12 Hz frequency band may be caused by the relatively homogeneous deeper layers in the lithosphere.

It has been shown that the temporal variations in Q_C^{-1} are closely related to stress changes, pore pressure, and medium heterogeneity in a complex pattern [28–31], thus providing critical constraints on the analysis of seismotectonics and hazard risks in a region. Three physical models have been proposed to explain these temporal variations. In the fractal model, coda attenuation is supposed to be caused by discrete scatters within the band-limited fractal random media to interpret the observed power-law frequency dependence of Q_C^{-1} at $f > 1$ Hz [32]. The value of n in $Q_c^{-1}(f) = Q{-}10f^{-n}$ is related to the fractal dimension D of three-dimensional heterogeneity by $D = 3\text{-}n/2$. It indicates that seismically active areas with greater n and greater Q_C^{-1} generally have smaller D. The resulted prediction relates the peak Q_C^{-1} precursor to various seismicity precursors derived from earthquake catalogs, indicating intensified clustering and localization of fractures and thus decrease in fractal dimension [33]. In the dilatancy-diffusion model, dilatancy or opening of cracks coupled with the Kaiser effect are assumed to cause pore pressure reduction and friction strength increase, thus leading to greater scattering and attenuation of seismic waves [34,35]. An increase in the frictional strength would also cause precursory seismic quiescence [36]. Another mechanism model for explaining the seismic quiescence is the creep model, in which preseismic stable slip leads to a stress decrease [37]. No quiescence tendency in the immediate hypocentral volume and decreased stress during the quiescence period favor the advantage of the creep model over dilatancy hardening [38]. Numerical experiments have demonstrated that quiescence only happens for events larger than the threshold magnitude determined by the critical weakening displacement [39]. The positive correlation between creep and seismicity may be attributed to the stress concentration caused by creep due to the finite size of a creeping crack [34]. Therefore, the temporal variations in Q_C^{-1} depend on the condition of aseismic fractures, which probably influences seismic fractures. The seismicity will increase for earthquakes with a size comparable to the scale length of creep fracture.

The observed temporal variations in Q_C^{-1} probably indicate differences in scattering or attenuation properties before and after the mainshock. In the vicinity of rupture region of the Wenchuan earthquake, the temporal variations in Q_C^{-1} can be reasonably described by the dilatancy model. The coseismically opened cracks act as seismic scatterers, leading to heterogeneities with dominant scale obtained from the wavelength of 1.25–3.5 Hz coda waves. The crack-related heterogeneities are assumed to cause increased scattering attenuation. It is supported by the consistency between the temporal Q_0^{-1} distribution and the coseismic volumetric strain change. These cracks can be forced to close by postseismic relaxation processes, such as crack healing, continuous pore pressure reduction by diffusion, and postseismic deformations lowering shear-stress concentrations [40]. The scattering attenuation is supposed to be a maximum when the wavelength of the seismic wave is comparable to twice the dominant scale length of heterogeneity. Taking an average S-wave velocity in the crust $V_S = 4.4$ km/s, the dominant scale of the heterogeneity is estimated to be $a = 0.6$–1.8 km at $f = 1.25$–3.5 Hz. It is noticeable that the effect of intrinsic absorption cannot be precluded from the observed Q_C^{-1} variations.

Next, the sensitivity of Q_C^{-1} on stress change of $d\tau$ associated with the earthquake will be discussed. The sensitivity can be described as $(-1/Q_C^{-1}) \times (dQ_C^{-1}/d\tau) = (1/Q_C) \times (dQ_C/d\tau)$ [9]. It can be inferred from Fig. 14 that post the mainshock, the maximum sensitivity for $f = 1.25$–24 Hz is estimated to be 37~50 $(\text{MPa})^{-1}$ for Longmenshan fault, 12–18 $(\text{MPa})^{-1}$ for the southern segment of Longmenshan fault, 30–35 $(\text{MPa})^{-1}$ for Sichuan Basin, corresponding to a static stress change of 0.01 MPa around the main rupture region. On the contrary, the maximum sensitivity for $f = 1.25$–24 Hz is estimated to be 10–28 $(\text{MPa})^{-1}$ for Songpan-Ganzi block, 10~38 $(\text{MPa})^{-1}$ for Chuan-Dian block, 12 $(\text{MPa})^{-1}$ for South China. For the 1995 Hyogo-ken Nanbu earthquake, the stress sensitivity of Q_C^{-1} around 3 and 4 Hz is estimated to be 10 $(\text{MPa})^{-1}$ [9]. For the 2011 Tohoku earthquake, the maximum sensitivity for $f = 1.25$ Hz is 12~16 MPa, corresponding to a static stress change of 0.01 MPa for the northern and southern borders of the source-rupture zone [41]. These values are much larger than the stress sensitivity of relative velocity change about 0.005 $(\text{MPa})^{-1}$ in the Longmenshan region [20]. The stress velocity coefficient was estimated to be 0.24 $(\text{MPa})^{-1}$ at 1 km by observing preseismic velocity changes from active source monitoring at the Parkfield SAFOD drill site [42].

The above discussion shows that the stress sensitivity of Q_C^{-1} variation is one order higher than that of seismic velocity. It indicates that Q_C^{-1} is a more sensitive indicator to stress change in the crust. Our results show that the influence of static stress change on coda attenuation around Longmenshan fault zone is larger than that in other relatively more stable blocks. It can further be inferred that the temporal variations in Q_c^{-1} for individual blocks are associated with significantly different physical mechanisms. These observations also suggest that the physical condition of the crust beneath Longmenshan fault zone is characterized by heterogeneity with a dominant scale of the order of a few kilometers enhanced by the static stress change induced by the Wenchuan earthquake. Furthermore, the heterogeneities responsible for enhanced scattering are crack related since only thin cracks can respond sensitively to a subtle stress change.

However, the dilatancy model cannot explain the complex temporal variations in Q_c^{-1} in the far field. The creep model is reasonable because of the most persistent observation on temporal change in Q_C^{-1}. From its apparent spatial correlation with the current seismicity, Q_C^{-1} is proposed to be a measure on the degree of aseismic fracture in the ductile part of the lithosphere. Monitoring temporal variations in Q_C^{-1} is critical to earthquake risk assessment due to the fact that the deformation in the ductile part contributes mainly to loading the brittle part. In addition, the near-fault postseismic deformation is attributed to aseismic fault slip while the far-field postseismic deformation is proposed to be mainly caused

by viscoelastic stress relaxation [40]. A precursory peak Q_C^{-1} is proposed to be caused by an increase in crack density in the ductile part of lithosphere due to creep activities followed by a localization of creep fractures near the failure site in the brittle part of lithosphere [43]. The preseismic decrease in Q_C^{-1} is probably attributed to creep fracture closure outside the localization area.

6. Conclusion

The analysis presented in our study has shown an increase in Q_C^{-1} by about 35%–45% in Longmenshan fault zone and 30%–35% in Sichuan Basin after the 2008 Wenchuan earthquake at lower frequencies of 1.25–8 Hz, which is confirmed by a statistical *t*-test at 95% confidence level. On the contrary, a decrease in the average Q_C^{-1} postseismic is observed by about 10%–18% in the southern segment of Longmenshan fault, 15%–38% in Chuan-Dian block, and 10–12% in South China block. No statistically significant change in Q_C^{-1} (<10%) is found in the Songpan-Ganzi block after the mainshock. Temporal variations in the average Q_C^{-1} in the individual blocks are significantly distinguishable during preseismic and postseismic period. It indicates a beacon to the change of tectonic static stress associated with the Wenchuan earthquake. Temporal variations of Q_C^{-1} in the vicinity of source rupture zone can be explained by the dilatancy model since heterogeneities responsible for enhanced scattering are crack related. The resulted characteristic scale length is estimated to be about 0.6–1.8 km. The sensitivity of Q_C^{-1} on the static stress change is evaluated to be the order of 0.01 $(\mathrm{MPa})^{-1}$ associated with the earthquake. The stress sensitivity of Q_C^{-1} is found to be one order higher than that of seismic velocity, indicating that Q_C^{-1} is a more sensitive indicator tostatic stress change in the crust. Our results also revealed that in the far field, the creep model is preferred for its ability to explain most of these significant observations. Q_C^{-1} is proposed to be a measure of creep fracture in the ductile part of lithosphere. Therefore, temporally monitoring Q_C^{-1} can provide a reliable indicator to static stress changes in the crust, which probably not lead to the occurrence of large earthquakes.

Author contributions

Junhua Hu: Conceptualization, Methodology, Software, Validation, Writing-Original Draft.
Guoxin Zhang: Supervision, Writing - Reviewing and Editing.
Liyun Fu: Funding acquisition, Formal analysis, Resources, Writing - Reviewing and Editing.
Yan Zhang: Visualization, Investigation, Data curation.
Songhui Li: Writing - Reviewing and Editing.

Conflicts of interest

The authors declare that there is no conflicts of interest.

Acknowledgment

This research is supported by the National Natural Science Foundation of China (No. 41874161 and No. 41720104006), the Youth Innovation Promotion Association Foundation of the Chinese Academy of Sciences (No. 2019069) and Guangdong Provincial Key R&D Program (No. 2019B111105002). Waveform data for this study are provided by Data Management Centre of China National Seismic Network at Institute of Geophysics (https://doi.org/10.11998/SeisDmc/SN,http://www.seisdmc.ac.cn/).

Appendices

Table A.1
Mean and standard deviations of Q_c^{-1} and the results of the statistical *t*-test for Each Period at the selected station network LMS

Frequency(Hz)	Period*	$\log_{10}(Q_C^{-1})$	σ^2	Number	*t*-test (%)
1.25	I	−1.8779	0.0760	287	100.00
1.25	II	−1.8154	0.0587	174	1.39
1.25	III	−1.6388	0.1682	247	0.00
1.75	I	−2.0366	0.0582	287	100.00
1.75	II	−1.9828	0.0439	174	1.52
1.75	III	−1.8114	0.1367	247	0.00
2.50	I	−2.2048	0.0464	287	100.00
2.50	II	−2.1602	0.0343	174	2.39
2.50	III	−1.9943	0.1119	247	0.00
3.50	I	−2.3634	0.0419	287	100.00
3.50	II	−2.3276	0.0310	174	5.56
3.50	III	−2.1669	0.0964	247	0.00
5.00	I	−2.5316	0.0441	287	100.00
5.00	II	−2.505	0.0337	174	16.77
5.00	III	−2.3498	0.0886	247	0.00
8.00	I	−2.7533	0.0581	287	100.00
8.00	II	−2.7388	0.0468	174	51.72
8.00	III	−2.5909	0.0917	247	0.00
12.00	I	−2.9445	0.0802	287	100.00
12.00	II	−2.9405	0.0670	174	88.07
12.00	III	−2.7988	0.1065	247	0.00
16.00	I	−3.0802	0.1015	287	100.00
16.00	II	−3.0837	0.0862	174	90.65
16.00	III	−2.9464	0.1240	247	0.00
20.00	I	−3.1854	0.1213	287	100.00
20.00	II	−3.1947	0.1039	174	77.59
20.00	III	−3.0608	0.1414	247	0.02
24.00	I	−3.2714	0.1395	287	100.00
24.00	II	−3.2854	0.1203	174	68.91
24.00	III	−3.1543	0.1582	247	0.05

* Three periods (I-III) during January 2007 to December 2008 for which the change in attenuation is estimated. "Number" represents number of events analyzed. The values of *t*-test less than 5.0 show statistically significant change with confidence level of 95.0%. The values of *t*-test equal 100 show statistically no change with confidence level of 95.0%.

Table A.2
Mean and standard deviations of Q_c^{-1} and the results of the statistical *t*-test for each period at the selected station network SB

Frequency(Hz)	Period*	$\log_{10}(Q_C^{-1})$	σ^2	Number	*t*-test (%)
1.25	I	−1.8529	0.0536	239	100
1.25	II	−1.8478	0.0554	158	82.98
1.25	III	−1.7208	0.1712	325	0.04
1.75	I	−2.0248	0.0387	239	100
1.75	II	−2.0153	0.0402	158	63.94
1.75	III	−1.8897	0.1450	325	0.01
2.50	I	−2.207	0.0299	239	100
2.50	II	−2.1928	0.0297	158	42.37
2.50	III	−2.0688	0.1234	325	0
3.50	I	−2.3789	0.0284	239	100
3.50	II	−2.3603	0.0250	158	27.14
3.50	III	−2.2378	0.1088	325	0
5.00	I	−2.5611	0.0338	239	100
5.00	II	−2.5379	0.0257	158	19.6
5.00	III	−2.4168	0.0995	325	0
8.00	I	−2.8012	0.0521	239	100
8.00	II	−2.7719	0.0353	158	17.99
8.00	III	−2.6528	0.0968	325	0
12.00	I	−3.0084	0.0781	239	100
12.00	II	−2.9737	0.0517	158	19.43
12.00	III	−2.8564	0.1034	325	0
16.00	I	−3.1553	0.1022	239	100
16.00	II	−3.1169	0.0678	158	20.88
16.00	III	−3.0009	0.1130	325	0.02
20.00	I	−3.2693	0.1241	239	100

(*continued on next page*)

Table A.2 (*continued*)

Frequency(Hz)	Period*	$\log_{10}(Q_C^{-1})$	σ^2	Number	*t*-test (%)
20.00	II	−3.228	0.0829	158	22.03
20.00	III	−3.1129	0.1233	325	0.04
24.00	I	−3.3625	0.1442	239	100
24.00	II	−3.3188	0.0968	158	22.95
24.00	III	−3.2045	0.1335	325	0.08

* Three periods (I-III) during January 2007 to December 2008 for which the change in attenuation is estimated. "Number" represents number of events analyzed. The values of *t*-test less than 5.0 show statistically significant change with confidence level of 95.0%. The values of *t*-test equal 100 show statistically no change with confidence level of 95.0%.

Table A.3
Mean and standard deviations of Q_c^{-1} and the Results of the Statistical *t*-test for each period at the selected station network SLMS

Frequency (Hz)	Period*	$\log_{10}(Q_C^{-1})$	σ^2	Number	*t*-test (%)
1.25	I	−1.8252	0.1133	376	100
1.25	II	−1.7738	0.0779	266	4.12
1.25	III	−1.8053	0.0751	775	10.73
1.75	I	−1.9983	0.0896	376	100
1.75	II	−1.9515	0.0629	266	3.75
1.75	III	−1.9713	0.0642	775	26.97
2.50	I	−2.1817	0.0740	376	100
2.50	II	−2.1398	0.0547	266	4.23
2.50	III	−2.1472	0.0578	775	66.24
3.50	I	−2.3548	0.0683	376	100
3.50	II	−2.3175	0.0542	266	6.35
3.50	III	−2.3132	0.0567	775	79.81
5.00	I	−2.5382	0.0718	376	100
5.00	II	−2.5059	0.0615	266	12.13
5.00	III	−2.4892	0.0608	775	34.08
8.00	I	−2.7799	0.0913	376	100
8.00	II	−2.7541	0.0833	266	27.8
8.00	III	−2.721	0.0744	775	9.3
12.00	I	−2.9885	0.1218	376	100
12.00	II	−2.9683	0.1132	266	46.38
12.00	III	−2.9211	0.0937	775	3.47
16.00	I	−3.1364	0.1512	376	100
16.00	II	−3.1202	0.1407	266	59.74
16.00	III	−3.063	0.1116	775	1.98
20.00	I	−3.2512	0.1783	376	100
20.00	II	−3.238	0.1655	266	69.36
20.00	III	−3.1731	0.1279	775	1.38
24.00	I	−3.3449	0.2034	376	100
24.00	II	−3.3343	0.1882	266	76.54
24.00	III	−3.263	0.1428	775	1.08

* Three periods (I-III) during January 2007 to December 2008 for which the change in attenuation is estimated. "Number" represents number of events analyzed. The values of *t*-test less than 5.0 show statistically significant change with confidence level of 95.0%. The values of *t*-test equal 100 show statistically no change with confidence level of 95.0%.

Table A.4
Mean and standard deviations of Q_c^{-1} and the results of the statistical *t*-test for each period at the selected station network SG

Frequency (Hz)	Period*	$\log_{10}(Q_C^{-1})$	σ^2	Number	*t*-test (%)
1.25	I	−1.833	0.0959	307	100
1.25	II	−1.8189	0.0787	238	58.38
1.25	III	−1.8157	0.0636	575	87.51
1.75	I	−2.0086	0.0710	307	100
1.75	II	−1.9843	0.0610	238	27.74
1.75	III	−1.9851	0.0491	575	96.27
2.50	I	−2.1947	0.0531	307	100
2.50	II	−2.1597	0.0491	238	7.42
2.50	III	−2.1647	0.0388	575	74.86
3.50	I	−2.3703	0.0442	307	100
3.50	II	−2.3251	0.0444	238	1.32
3.50	III	−2.3342	0.0338	575	54.17
5.00	I	−2.5564	0.0432	307	100
5.00	II	−2.5005	0.0463	238	0.22
5.00	III	−2.5138	0.0335	575	37.28
8.00	I	−2.8017	0.0552	307	100
8.00	II	−2.7316	0.0596	238	0.07
8.00	III	−2.7504	0.0411	575	25.74
12.00	I	−3.0133	0.0776	307	100
12.00	II	−2.9309	0.0809	238	0.07
12.00	III	−2.9546	0.0548	575	22.01
16.00	I	−3.1635	0.1004	307	100
16.00	II	−3.0724	0.1017	238	0.1
16.00	III	−3.0994	0.0687	575	21.02
20.00	I	−3.2799	0.1220	307	100
20.00	II	−3.1821	0.1209	238	0.12
20.00	III	−3.2118	0.0817	575	20.72
24.00	I	−3.3751	0.1421	307	100
24.00	II	−3.2717	0.1387	238	0.15
24.00	III	−3.3036	0.0938	575	20.67

* Three periods (I-III) during January 2007 to December 2008 for which the change in attenuation is estimated. "Number" represents number of events analyzed. The values of *t*-test less than 5.0 show statistically significant change with confidence level of 95.0%. The values of *t*-test equal 100 show statistically no change with confidence level of 95.0%.

Table A.5
Mean and standard deviations of Q_c^{-1} and the results of the statistical *t*-test for each period at the selected station network CD

Frequency(Hz)	Period*	$\log_{10}(Q_C^{-1})$	σ^2	Number	*t*-test (%)
1.25	I	−1.8409	0.0675	118	100
1.25	II	−1.879	0.0392	56	33.27
1.25	III	−1.9509	0.0844	140	9.08
1.75	I	−2.0033	0.0533	118	100
1.75	II	−2.0257	0.0325	56	52.5
1.75	III	−2.1117	0.0631	140	2.06
2.50	I	−2.1756	0.0439	118	100
2.50	II	−2.1812	0.0296	56	86.24
2.50	III	−2.2823	0.0470	140	0.21
3.50	I	−2.3381	0.0404	118	100
3.50	II	−2.3279	0.0310	56	74.53
3.50	III	−2.4431	0.0379	140	0.02
5.00	I	−2.5103	0.0422	118	100
5.00	II	−2.4834	0.0367	56	41.03
5.00	III	−2.6136	0.0348	140	0
8.00	I	−2.7373	0.0536	118	100
8.00	II	−2.6883	0.0510	56	19.04
8.00	III	−2.8383	0.0409	140	0
12.00	I	−2.9331	0.0715	118	100
12.00	II	−2.8651	0.0695	56	11.71
12.00	III	−3.0322	0.0556	140	0
16.00	I	−3.072	0.0887	118	100
16.00	II	−2.9905	0.0861	56	9.19
16.00	III	−3.1697	0.0712	140	0.01
20.00	I	−3.1798	0.1047	118	100
20.00	II	−3.0878	0.1009	56	7.98
20.00	III	−3.2764	0.0863	140	0.01
24.00	I	−3.2679	0.1194	118	100
24.00	II	−3.1673	0.1143	56	7.28
24.00	III	−3.3636	0.1006	140	0.02

* Three periods (I-III) during January 2007 to December 2008 for which the change in attenuation is estimated. "Number" represents number of events analyzed. The values of *t*-test less than 5.0 show statistically significant change with confidence level of 95.0%. The values of *t*-test equal 100 show statistically no change with confidence level of 95.0%.

Table A.6
Mean and standard deviations of Q_c^{-1} and the results of the statistical *t*-test for each period at the selected station network SC

Frequency (Hz)	Period*	$\log_{10}(Q_C^{-1})$	σ^2	Number	*t*-test (%)
1.25	I	−1.8574	0.0730	322	100
1.25	II	−1.7929	0.0764	211	0.77
1.25	III	−1.8512	0.0484	555	0.24
1.75	I	−2.0122	0.0570	322	100
1.75	II	−1.9541	0.0599	211	0.67
1.75	III	−2.0126	0.0392	555	0.07
2.50	I	−2.1762	0.0472	322	100
2.50	II	−2.125	0.0496	211	0.86
2.50	III	−2.1837	0.0329	555	0.02
3.50	I	−2.331	0.0448	322	100
3.50	II	−2.2862	0.0466	211	1.82
3.50	III	−2.3452	0.0302	555	0.01
5.00	I	−2.4951	0.0495	322	100
5.00	II	−2.4572	0.0506	211	5.61
5.00	III	−2.5163	0.0307	555	0.01
8.00	I	−2.7112	0.0671	322	100
8.00	II	−2.6824	0.0672	211	20.92
8.00	III	−2.7418	0.0369	555	0.06
12.00	I	−2.8977	0.0926	322	100
12.00	II	−2.8767	0.0917	211	43.45
12.00	III	−2.9363	0.0472	555	0.26
16.00	I	−3.03	0.1166	322	100
16.00	II	−3.0145	0.1149	211	60.73
16.00	III	−3.0743	0.0572	555	0.64
20.00	I	−3.1327	0.1386	322	100
20.00	II	−3.1215	0.1362	211	73.3
20.00	III	−3.1814	0.0666	555	1.16
24.00	I	−3.2165	0.1587	322	100
24.00	II	−3.2088	0.1557	211	82.65
24.00	III	−3.2689	0.0754	555	1.77

* Three periods (I-III) during January 2007 to December 2008 for which the change in attenuation is estimated. "Number" represents number of events analyzed. The values of *t*-test less than 5.0 show statistically significant change with confidence level of 95.0%. The values of *t*-test equal 100 show statistically no change with confidence level of 95.0%.

Table A.7
Mean and standard deviations of Q_c^{-1} and the results of the statistical *t*-test for each period at the selected station network XJH

Frequency (Hz)	Period*	$\log_{10}(Q_C^{-1})$	σ^2	Number	*t*-test (%)
1.25	I	−1.8745	0.0756	129	100
1.25	II	−1.7967	0.0927	79	5.87
1.25	III	−1.9482	0.0551	231	0
1.75	I	−2.0334	0.0580	129	100
1.75	II	−1.9766	0.0673	79	11.06
1.75	III	−2.0928	0.0403	231	0.01
2.50	I	−2.2018	0.0462	129	100
2.50	II	−2.1673	0.0506	79	27.1
2.50	III	−2.2461	0.0301	231	0.14
3.50	I	−2.3607	0.0416	129	100
3.50	II	−2.3472	0.0447	79	64.83
3.50	III	−2.3907	0.0258	231	5.76
5.00	I	−2.5291	0.0436	129	100
5.00	II	−2.5379	0.0488	79	77.37
5.00	III	−2.5439	0.0268	231	79.79
8.00	I	−2.7511	0.0570	129	100
8.00	II	−2.7892	0.0704	79	28.52
8.00	III	−2.7459	0.0370	231	12.01
12.00	I	−2.9425	0.0784	129	100
12.00	II	−3.006	0.1039	79	13.6
12.00	III	−2.9201	0.0538	231	1.11
16.00	I	−3.0784	0.0992	129	100
16.00	II	−3.1598	0.1360	79	9.17
16.00	III	−3.0438	0.0702	231	0.27
20.00	I	−3.1838	0.1184	129	100
20.00	II	−3.2791	0.1657	79	7.21
20.00	III	−3.1396	0.0855	231	0.11
24.00	I	−3.2699	0.1362	129	100
24.00	II	−3.3766	0.1930	79	6.14
24.00	III	−3.218	0.0997	231	0.06

(*continued on next page*)

Table A.7 (*continued*)

* Three periods (I-III) during January 2007 to December 2008 for which the change in attenuation is estimated. "Number" represents number of events analyzed. The values of *t*-test less than 5.0 show statistically significant change with confidence level of 95.0%. The values of *t*-test equal 100 show statistically no change with confidence level of 95.0%.

Table A.8
Mean and standard deviations of Q_c^{-1} and the Results of the Statistical *t*-test for each period at the selected station network XSH

Frequency (Hz)	Period*	$\log_{10}(Q_C^{-1})$	σ^2	Number	*t*-test (%)
1.25	I	−1.771	0.0865	167	100
1.25	II	−1.8245	0.0742	131	10.8
1.25	III	−1.8641	0.0707	317	15.55
1.75	I	−1.9447	0.0681	167	100
1.75	II	−1.9839	0.0604	131	18.78
1.75	III	−2.0169	0.0536	317	17.8
2.50	I	−2.1288	0.0585	167	100
2.50	II	−2.1527	0.0523	131	38.55
2.50	III	−2.1788	0.0412	317	23.39
3.50	I	−2.3025	0.0589	167	100
3.50	II	−2.3121	0.0507	131	72.73
3.50	III	−2.3316	0.0349	317	34.42
5.00	I	−2.4866	0.0692	167	100
5.00	II	−2.481	0.0556	131	84.71
5.00	III	−2.4936	0.0339	317	54.53
8.00	I	−2.7292	0.0983	167	100
8.00	II	−2.7035	0.0722	131	45.48
8.00	III	−2.707	0.0415	317	88.22
12.00	I	−2.9386	0.1377	167	100
12.00	II	−2.8955	0.0959	131	28.63
12.00	III	−2.8911	0.0563	317	87
16.00	I	−3.0871	0.1737	167	100
16.00	II	−3.0317	0.1179	131	22.03
16.00	III	−3.0217	0.0714	317	74.07
20.00	I	−3.2023	0.2061	167	100
20.00	II	−3.1374	0.1380	131	18.63
20.00	III	−3.123	0.0857	317	66.35
24.00	I	−3.2964	0.2356	167	100
24.00	II	−3.2237	0.1563	131	16.56
24.00	III	−3.2058	0.0992	317	61.25

* Three periods (I-III) during January 2007 to December 2008 for which the change in attenuation is estimated. "Number" represents number of events analyzed. The values of *t*-test less than 5.0 show statistically significant change with confidence level of 95.0%. The values of *t*-test equal 100 show statistically no change with confidence level of 95.0%.

References

[1] P.Z. Zhang, X.Z. Wen, Z.K. Shen, J.H. Chen, Oblique, high-angle, listric-reverse faulting and associated development of strain: the Wenchuan earthquake of May 12, 2008, Sichuan, China, Annu. Rev. Earth Planet Sci. 38 (1) (2010) 353–382, https://doi.org/10.1146/annurev-earth-040809-152602.

[2] T. Parsons, C. Ji, E. Kirby, Stress changes from the 2008 Wenchuan earthquake and increased hazard in the Sichuan basin, Nature 454 (7203) (2008) 509–510, https://doi.org/10.1038/nature07177.

[3] A. Yin, A special issue on the great 12 May 2008 Wenchuan earthquake (Mw 7.9): observations and unanswered questions, Tectonophysics 491 (1) (2010) 1–9, https://doi.org/10.1016/j.tecto.2010.05.019.

[4] M. Naghavi, H. Rahimi, A. Moradi, S. Mukhopadhyay, Spatial variations of seismic attenuation in the North West of Iranian plateau from analysis of coda waves, Tectonophysics 708 (2017) 70–80, https://doi.org/10.1016/j.tecto.2017.04.026.

[5] K. Aki, B. Chouet, Origin of coda waves: source, attenuation, and scattering effects, J. Geophys. Res. 80 (23) (1975) 3322–3342, https://doi.org/10.1029/JB080i023p03322.

[6] M. Farrokhi, H. Hamzehloo, H. Rahimi, M. Allameh Zadeh, Separation of intrinsic and scattering attenuation in the crust of central and eastern Alborz region, Iran, Phys. Earth Planet. In. 253 (2016) 88–96, https://doi.org/10.1016/j.pepi.2016.02.005.

[7] V. Wong, C.J. Rebollar, L. Munguía, Attenuation of coda waves at the tres virgenes volcanic area, baja California sur, Mexico, Bull. Seismol. Soc. Am. 91 (6) (2001) 1936, https://doi.org/10.1785/0120010223, 1936.

[8] H. Sato, Temporal change in attenuation intensity before and after the eastern yamanashi earthquake of 1983 in central Japan, J. Geophys. Res.: Solid Earth 91 (B2) (1986) 2049–2061, https://doi.org/10.1029/JB091iB02p02049.
[9] Y. Hiramatsu, N. Hayashi, M. Furumoto, H. Katao, Temporal changes in coda Q^{-1} and b value due to the static stress change associated with the 1995 Hyogo-ken Nanbu earthquake, J. Geophys. Res.: Solid Earth 105 (B3) (2000) 6141–6151, https://doi.org/10.1029/1999JB900432.
[10] J.Y. Peng, K. Aki, B. Chouet, P. Johnson, W.H.K. Lee, S. Marks, J.T. Newberry, A.S. Ryall, S.W. Stewart, D.M. Tottingham, Temporal change in coda associated with the round valley, California, earthquake of november 23, 1984, J. Geophys. Res.: Solid Earth 92 (B5) (1987) 3507–3526, https://doi.org/10.1029/JB092iB05p03507.
[11] G.A. Tselentis, Temporal variation of body wave attenuation as related to two earthquake doublets in W. Greece, Pure Appl. Geophys. 140 (1) (1993) 49–62, https://doi.org/10.1007/BF00876870.
[12] G.C. Beroza, A.T. Cole, W.L. Ellsworth, Stability of coda wave attenuation during the Loma Prieta, California, earthquake sequence, J. Geophys. Res.: Solid Earth 100 (B3) (1995) 3977–3987, https://doi.org/10.1029/94JB02574.
[13] G.A. Tselentis, Evidence for stability in coda Q associated with the Egion (Central Greece) earthquake of 15 June 1995, Bull. Seismol. Soc. Am. 87 (6) (1997) 1679–1684, https://doi.org/10.1016/S0009-2541(97)00104-6.
[14] A. Jin, K. Aki, Spatial and temporal correlation between coda Q^{-1} and seismicity and its physical mechanism, J. Geophys. Res.: Solid Earth 94 (B10) (1989) 14041–14059, https://doi.org/10.1029/JB094iB10p14041.
[15] D.A. Novelo-Casanova, E. Berg, V. Hsu, C.E. Helsley, Time-space variation of seismic S-wave coda attenuation (Q_c^{-1}) and magnitude distribution (b-values) for the Petatlan Earthquake, Geophys. Res. Lett. 12 (11) (1985) 789–792, https://doi.org/10.1029/GL012i011p00789.
[16] M. Fehler, P. Roberts, T. Fairbanks, A temporal change in coda wave attenuation observed during an eruption of Mount St. Helens, J. Geophys. Res.: Solid Earth 93 (B5) (1988) 4367–4373, https://doi.org/10.1029/JB093iB05p04367.
[17] Q.Y. Liu, Y. Li, J.H. Chen, B. Guo, S.H. Qi, Wenchuan M_S8.0 earthquake: preliminary study of the S-wave velocity structure of the crust and upper mantle, Chin. J. Geophys. 52 (2) (2009) 309–319.
[18] A. Obermann, B. Froment, M. Campillo, E. Larose, T. Planès, B. Valette, J.H. Chen, Q.Y. Liu, Seismic noise correlations to image structural and mechanical changes associated with the Mw7.9 2008 Wenchuan earthquake, J. Geophys. Res.: Solid Earth 119 (4) (2014) 3155–3168, https://doi.org/10.1002/2013JB010932.
[19] X.Z. Yin, J.H. Chen, Z. Peng, X. Meng, Q.Y. Liu, B. Guo, S.C. Li, Evolution and distribution of the early aftershocks following the 2008 Mw 7.9 Wenchuan earthquake in Sichuan, China, J. Geophys. Res.: Solid Earth 123 (9) (2018) 7775–7790, https://doi.org/10.1029/2018JB015575.
[20] J.H. Chen, B. Froment, Q.Y. Liu, M. Campillo, Distribution of seismic wave speed changes associated with the 12 May 2008 M_w 7.9 Wenchuan earthquake, Geophys. Res. Lett. 37 (18) (2010) 109–118, https://doi.org/10.1029/2010GL044582.
[21] Q.D. Deng, Y. Ran, X. Yang, W. Min, Q. Chu, Active Tectonics Map of China, Earthquake Press, Beijing, 2007.
[22] H. Sato, Single isotropic scattering model including wave conversions simple theoretical model of the short period body wave propagation, J. Phys. Earth 25 (2) (1977) 163–176, https://doi.org/10.4294/jpe1952.25.163.
[23] J.J. Pulli, Attenuation of coda waves in new england, Bull. Seismol. Soc. Am. 74 (4) (1984) 1149–1166, https://doi.org/10.1016/0040-1951(85)90292-6.
[24] M. Tsujiura, Spectral analysis of the coda waves from local earthquakes, Bullet. Earthquake Res. Inst. University Tokyo 53 (1) (1978) 1–48.
[25] M. Takahara, K. Yomogida, Estimation of coda Q using the maximum likelihood method, Pure Appl. Geophys. 139 (2) (1992) 255–268, https://doi.org/10.1007/BF00876330.
[26] Z.X. Huang, M. Wyss, Coda Q before the 1983 Hawaii (M_S = 6.6) earthquake, Bull. Seismol. Soc. Am. 78 (3) (1988) 1279–1296, https://doi.org/10.1016/0040-1951(88)90183-7.
[27] J.S. Lei, D.P. Zhao, Structural heterogeneity of the Longmenshan fault zone and the mechanism of the 2008 Wenchuan earthquake (M_s 8.0), G-cubed 10 (10) (2009), https://doi.org/10.1029/2009gc002590.
[28] M. Murru, C. Montuori, M. Wyss, E. Privitera, The locations of magma chambers at Mt. Etna, Italy, mapped by b-values, Geophys. Res. Lett. 26 (16) (1999) 2553–2556, https://doi.org/10.1029/1999GL900568.
[29] S. Wiemer, M. Baer, Mapping and removing quarry blast events from seismicity catalogs, Bull. Seismol. Soc. Am. 90 (2) (2000) 525–530, https://doi.org/10.1785/0119990104.
[30] S. Wiemer, K. Katsumata, Spatial variability of seismicity parameters in aftershock zones, J. Geophys. Res.: Solid Earth 104 (B6) (1999) 13135–13151, https://doi.org/10.1029/1999JB900032.
[31] M. Wyss, K. Shimazaki, S. Wiemer, Mapping active magma chambers by b values beneath the off-Ito volcano, Japan, J. Geophys. Res.: Solid Earth 102 (B9) (1997) 20413–20422, https://doi.org/10.1029/97JB01074.
[32] H. Sato, Temporal change in scattering and attenuation associated with the earthquake occurrence—a review of recent studies on coda waves, Pure Appl. Geophys. 126 (2–4) (1988) 465–497, https://doi.org/10.1029/SP032p0054.
[33] R.E. Habermann, Precursory seismic quiescence: past, present, and future, Pure Appl. Geophys. 126 (2) (1988) 279–318, https://doi.org/10.1007/BF00879000.
[34] D. Andrews, Coupling of energy between tectonic processes and earthquakes, J. Geophys. Res.: Solid Earth 83 (B5) (1978) 2259–2264, https://doi.org/10.1029/JB083iB05p02259.
[35] C.H. Scholz, Mechanisms of seismic quiescences, Pure Appl. Geophys. 126 (2) (1988) 701–718, https://doi.org/10.1007/BF00879016.
[36] T. Tsukuda, Coda-Q before and after the 1983 misasa earthquake of M 6.2, tottori prefecture, Japan, Pure Appl. Geophys. 128 (1) (1988) 261–279, https://doi.org/10.1007/BF01772600.
[37] W.D. Stuart, Strain softening prior to two-dimensional strike slip earthquakes, J. Geophys. Res.: Solid Earth 84 (B3) (1979) 1063–1070, https://doi.org/10.1029/JB084iB03p01063.
[38] M. Wyss, R.E. Habermann, Precursory seismic quiescence, Pure Appl. Geophys. 126 (2) (1988) 319–332, https://doi.org/10.1007/BF00879001.
[39] T. Cao, K. Aki, Seismicity simulation with a mass-spring model and a displacement hardening-softening friction law, Pure Appl. Geophys. 122 (1) (1984) 10–24, https://doi.org/10.1007/BF00879646.
[40] Z. Shao, R. Wang, Y. Wu, L. Zhang, Rapid afterslip and short-term viscoelastic relaxation following the 2008 M_W 7.9 Wenchuan earthquake, Earthq. Sci. 24 (2) (2011) 163–175, https://doi.org/10.1007/s11589-010-0781-z.
[41] S. Hiratsuka, T. Sato, Alteration of stress field brought about by the occurrence of the 2011 off the Pacific coast of Tohoku Earthquake (Mw 9.0), Earth Planet. Space 63 (7) (2011) 681–685, https://doi.org/10.5047/eps.2011.05.013.
[42] F. Niu, P.G. Silver, T.M. Daley, X. Cheng, E.L. Majer, Preseismic velocity changes observed from active source monitoring at the Parkfield SAFOD drill site, Nature 454 (7201) (2008) 204–208, https://doi.org/10.1038/nature07111.
[43] F. Su, K. Aki, Temporal and spatial variation on coda Q_{-1} associated with the North Palm Springs earthquake of July 8, 1986, Pure Appl. Geophys. 133 (1) (1990) 23–52, https://doi.org/10.1007/BF00876701.

Junhua Hu received the Ph.D. degree in Geophysics from Institute of Geology and Geophysics, Chinese Academy of Sciences, in 2018. He is working as a postdoctor with China Institute of Water Resources and Hydropower Research. His main research interests include seismology method, earthquake mechanism and risk evaluation, seismic and electromagnetic exploration. His current research focuses on seismic wave scattering, coda waves and ambient noise. His research has been supported by several projects of the National Natural Science Foundation of China.

Guoxin Zhang received the Ph.D. degree in high dam and large structure from the Department of hydraulic engineering, Tsinghua University in 1989. He was the director of Department of Structures and Materials in China Institute of Water Resources and Hydropower Research from 2001 to 2020. He is also the director of National Research and Development Center for efficient utilization of hydropower energy and dam safety, director of China Office of International Institute of hydropower (IHA), Deputy Secretary General of China Society of dam engineering, and director of hydraulic structure special committee of China Society of water resources. He mainly engaged in numerical calculation method, numerical analysis of hydraulic structure, temperature stress and temperature control of concrete dam.

Liyun Fu received the B.S. degree in petroleum exploration from Chengdu University of Technology, Chengdu, China, in 1985, and the M.S. and Ph.D. degrees in geophysics from the China University of Petroleum, Beijing, China, in 1992 and 1995, respectively. From 1995 to 1997, he was a Postdoctoral fellow of engineering mechanics in the Tsinghua University. From 1997 to 1999, he was a Postdoctoral fellow of tectonic structure in the University of California at Los Angeles (UCLA). From 1999 to 2004, he was a Research Scientist in the Commonwealth Scientific and Industrial Research Organization (CSIRO) and the Australian Resources Research Centre, and simultaneously, he was also a Visiting Professor at the College of Physics, Curtin University, Australia. From 2002 to 2003 he was a Visiting Researcher in the Institute of Geophysics and Planetary Physics (IGPP) at UCLA. From 2004 to 2017, he was the Group Leader of seismology at the Institute of Geology and Geophysics, Chinese Academy of Sciences, Beijing, China. Since 2017, he has been a Professor with the School of Geosciences, China University of Petroleum (East China), Qingdao, China. His research interests include regional seismic facies, crustal seismic wave propagation, seismic simulation and imaging of complex geological structures.

Yan Zhang received the M.S. degree in Geophysics from the Institution of Geophysics, China Earthquake Administration in 2010 and the Ph.D. degree from the Institute of Geology and Geophysics, Chinese Academy of Sciences in 2014. She worked as a Post-doctor in the institute from 2014.6 to 2016.12.He is currently an Associate Professor with the Institute of Geology and Geophysics. Her research interests include Hydro-seismology and Rock-physics. She gained the 2016 Outstanding Paper Award of the "Earth and Planets" National Postdoctoral Academic Forum. Her research has been supported by several projects of the National Natural Science Foundation of China and Strategic Priority Research Program of the Chinese Academy of Sciences.

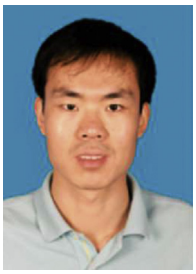

Songhui Li obtained the Ph.D. degree in engineering and is working as a professor level senior engineer in Department of Structures and Materials in China Institute of Water Resources and Hydropower Research. His main research fields include water conservancy engineering information construction, concrete temperature control and crack prevention, intelligent monitoring of concrete dam, numerical simulation on complex hydraulic structure, defect detection and damage diagnosis of hydraulic structure. As the project leader or scientific research backbone, he participated in the national "11th Five Year Plan" and "12th Five Year Plan" science and technology support projects, and more than 10 national key natural science foundation projects. He has won 8 provincial and ministerial awards for scientific and technological progress (including 2 special awards, 2 first prizes and 3 s prizes), published more than 30 academic papers, applied for 51 invention patents (30 authorized), published 1 monograph and 1 standard.